Cite as: A. Rialdi *et al.*, *Science* 10.1126/science.aad7993 (2016).

Topoisomerase 1 inhibition suppresses inflammatory genes and protects from death by inflammation

Alex Rialdi,[1,2]* Laura Campisi,[1,2]* Nan Zhao,[1,2] Arvin Cesar Lagda,[1,2] Colette Pietzsch,[3] Jessica Sook Yuin Ho,[4] Luis Martinez-Gil,[1,5] Romain Fenouil,[6] Xiaoting Chen,[7] Megan Edwards,[1] Giorgi Metreveli,[1,2] Stefan Jordan,[8] Zuleyma Peralta,[6] Cesar Munoz-Fontela,[9] Nicole Bouvier,[1] Miriam Merad,[8] Jian Jin,[10] Matthew Weirauch,[7] Sven Heinz,[11,12] Chris Benner,[12] Harm van Bakel,[6] Chris Basler,[1] Adolfo García-Sastre,[1,2] Alexander Bukreyev,[3] Ivan Marazzi[1,2]†

[1]Department of Microbiology, Icahn School of Medicine at Mount Sinai, New York, NY 10029, USA. [2]Global Health and Emerging Pathogens Institute, Icahn School of Medicine at Mount Sinai, New York, NY 10029, USA. [3]Department of Pathology, Microbiology, and Immunology, University of Texas Medical Branch, Galveston, TX 77555, USA. [4]Laboratory of Methyltransferases in Development and Disease, Institute of Molecular and Cell Biology, Singapore. [5]Department of Biochemistry and Molecular Biology, Universitat de Valencia, Valencia, Spain. [6]Icahn Institute for Genomics and Multiscale Biology, Icahn School of Medicine at Mount Sinai, New York, NY 10029, USA. [7]Center for Autoimmune Genomics and Etiology (CAGE) and Divisions of Biomedical Informatics and Developmental Biology, Cincinnati Children's Hospital Medical Center, Cincinnati, OH 45229, USA. [8]Department of Oncological Sciences, Tisch Cancer Institute and Immunology Institute, Icahn School of Medicine at Mount Sinai, New York, NY 10029, USA. [9]Heinrich Pette Institute, Leibniz Institute for Experimental Virology, Hamburg, Germany. [10]Department of Structural and Chemical Biology, Department of Oncological Sciences, and Department of Pharmacology and Systems Therapeutics, Icahn School of Medicine at Mount Sinai, New York, NY 10029, USA. [11]Department of Cellular and Molecular Medicine, University of California, San Diego, 9500 Gilman Drive, La Jolla, CA 92093, USA. [12]Salk Institute for Biological Studies, 10010 North Torrey Pines Road, La Jolla, CA 92037, USA.

*These authors contributed equally to this work.

†Corresponding author. Email: ivan.marazzi@mssm.edu

The host innate immune response is the first line of defense against pathogens and is orchestrated by the concerted expression of genes induced by microbial stimuli. Deregulated expression of these genes is linked to the initiation and progression of diseases associated with exacerbated inflammation. Here, we identify Topoisomerase 1 (Top1) as a positive regulator of RNA polymerase II (RNAPII) transcriptional activity at pathogen-induced genes. Depletion or chemical inhibition of Top1 suppresses the host response against Influenza and Ebola viruses as well as bacterial products. As a result, therapeutic pharmacological inhibition of Top1 protects mice from death in experimental models of lethal inflammation. Our results indicate that Top1 inhibition could be used as therapy against life threatening infections characterized by an acutely exacerbated immune response.

The innate immune response is a key defense mechanism against infections. Activation of innate immune cells relies on the expression of a large family of Pattern Recognition Receptors (PRRs), which detect distinct conserved microbial structures, called Pathogen-Associated Molecular Patterns (PAMPs) (*1*, *2*). The immunological response that follows PRR downstream signaling is then governed by the combinatorial expression of PAMP-response genes (*3*).

While the function of many of the PAMP-response genes and their antiviral/inflammatory activity still remains elusive, their expression is essential for the host defense against pathogens (*4*). Failure in regulating the induction, and post-induction repression of these anti-microbial genes can alter the balance between pro- and anti-inflammatory states, often leading to detrimental effects for the host (*5*–*7*). Indeed, hyper activation of anti-microbial genes has been suggested to be responsible for the high mortality rates during highly pathogenic infections (*8*, *9*). Another well-known example is the syndrome called "septic shock," where the uncontrolled expression of pro-inflammatory genes in response to bacterial PAMPs leads to severe collateral effects, such as local and systemic tissue injury, which can often be lethal to the host (*10*). In these contexts, pharmacological inhibition of factors that control the magnitude of the innate immune response could be useful for therapy.

Here, we show that the enzyme Topoisomerase 1 (Top1) exerts an activating role on the transcriptional response against infection in both cells and at the organismal level. This effect is achieved via Top1-assisted transcriptional activation of pro-inflammatory genes.

We demonstrate that chemical inhibition, as well as reduced expression of Top1, limits the overexpression of inflammatory genes characteristic of infection with influenza and Ebola viruses and bacterial products. Notably, Top1 inhibition rescues mortality in mouse models of lethal inflammation caused by overexposure to bacterial PAMPs. Our

results suggest the therapeutic usage of Top1 inhibitors for the treatment of diseases characterized by exacerbated innate immune responses.

Topoisomerase 1 promotes PAMP-induced gene expression

Our goal was to identify novel regulatory mechanisms controlling the transcriptional response to pathogens by the innate immune system. We designed a reporter assay to compare the potency of the transcriptional response to viral PAMPs and its dependence on a chromatin environment (fig. S1A). We utilized both the influenza A virus strain PR8ΔNS1 and Sendai virus since they are known to be strong inducers of PAMP-mediated gene expression (fig. S1C) (*11*). We then selected nine chemical inhibitors (fig. S1B) with already known or inferred chromatin targets and gauged their activity at various concentrations (fig. S1C) (*12–20*).

Our analysis revealed that flavopiridol (FVD), (+)-JQ1 and camptothecin (CPT) effectively inhibit the interferon-beta (IFN-β)-driven transcription from chromatinized templates (Fig. 1A and fig. S1C). These observations were further reinforced by the efficacy of the three compounds to suppress the endogenous expression of two key PAMP-induced genes, IFN-β and IFN-induced protein with tetratricopeptide repeats 1 (IFIT1) in the human lung epithelial cell line A549, at early (4 hours) and late (12 hours) time points following PR8ΔNS1 virus infection (Fig. 1B). Notably, our analysis was performed using all of the compounds at concentrations that do not induce cytotoxicity in treated cells (fig. S1D).

The cellular targets of FVD, (+)-JQ-1 and CPT are P-TEFb (the inhibitor of Positive Transcription Elongation Factor b), BET proteins (Bromodomain and Extra-Terminal motif), and Top1 (Topoisomerase 1), respectively (*20–22*). P-TEFb, BET proteins and Top1 are ubiquitously expressed, and thought to control basal transcriptional levels of many genes. However, recent studies showed that P-TEFb and BET protein inhibitors have a specific effect on genes induced by innate immune stimuli (*23*) and during oncogenic transformation (*24*), highlighting their usage in what is often referred to as epigenetic therapy (*25*). For this reason, our observation that FVD and (+)-JQ-1 suppress PAMP-induced genes, as well as the validation that such an effect is phenocopied by small interfering RNA (siRNA)-mediated depletion of their cellular targets (fig. S2), was not surprising. In contrast, the impact of CPT treatment on PAMP-induced genes, though previously observed (*26–28*), was less expected in light of recent genome-wide analyses demonstrating that Top1 inhibition suppresses the expression of the majority of long genes (>100Kb) while inducing a fraction of smaller genes (*29*, *30*). The inhibitory effect at long genes is believed to be caused by Top1-mediated resolution of topological constraints occurring on long templates as a result of RNA polymerase II (RNAPII) activity (*29*, *31*). The activating effect is instead thought to be dependent on gene-specific features like topology, promoter sequence, or indirect effects (*30–33*). A concentration-dependent effect of the inhibitor CPT is also known, whereby high concentration and prolonged treatment leads to DNA damage (*34*).

To analyze in our system the role of Top1 per se, i.e., independently of its chemical inhibition, we examined the effect of transient Top1 depletion via small interfering RNA (siRNA). We infected control (siCtrl) and Top1-depleted (siTop1) A549 cells with influenza PR8ΔNS1 virus and assessed global differences in gene expression by microarray analysis (Fig. 1C, fig. S3, and table S1). Upon infection, Top1 depletion significantly decreased expression of 84 genes in infected cells as compared to the control (siCtrl) (Fig. 1C). Remarkably, none of the downregulated genes were long but they were highly enriched for transcripts coding for inflammatory cytokines and interferon stimulated genes (ISGs) (Fig. 1C, fig. S3, A and B, and table S2). Importantly, the expression of housekeeping genes was unaffected independently of their level of expression (fig. S3C) indicating that Top1 depletion does not suppress gene expression 'tout court' but predominantly affects genes induced in response to infection. Notably, our gene knockdown experiments rule out the possibility that the suppression of PAMP-induced genes that we observed is the consequence of CPT-mediated stabilization of covalent complexes or induced cell damage, which are known to be caused by high dosage and prolonged chemical inhibition of Top1 (fig. S1D) (*29*). To strengthen this point, we performed a wash-out experiment in the presence and absence of Top1 inhibition. As shown in Fig. 1D, the effect of Top1 inhibition on inflammatory genes was fully reversible upon drug wash-out, indicating the absence of any permanent change or damage in treated cells.

We then performed a global proteomic analysis in influenza virus infected A549 cells in the presence and absence of CPT treatment. Mass spectrometry analysis indicates that the protein levels of PAMP-induced genes were compromised upon Top1 inhibition (Fig. 1E), as indicated by the representative proteins DEAD (Asp-Glu-Ala-Asp) Box Polypeptide 60-Like (DDX60L), Interferon-Induced Protein With Tetratricopeptide Repeats 3 (IFIT3), 2′-5′ oligoadenylate synthetase (OAS) and NFBKIE. Importantly, the production of housekeeping proteins was unaffected independently of their expression level [(Fig. 1E, low expressed: HPRT, (hypoxanthine-guanine phosphoribosyltransferase), high expressed: ACTB (β-actin,)]. Overall, these results indicate that Top1 is required to up-regulate antiviral gene expression after recognition of viral PAMPs.

Top1 controls RNAPII activity at PAMP-induced gene loci

To confirm the specificity of Top1 activity in our system, we first investigated whether the inhibition of PAMP-induced genes could be reproduced using a different Top1 inhibitor. We therefore used topotecan (TPT), a Food and Drug Administration (FDA)-approved Top1 inhibitor. Our results indicate that both CPT and TPT suppress virus-induced genes (Fig. 2A) and not viral entry or replication (fig. S4). This was further supported by the observed PAMP-induced gene suppression in response to infection with Sendai virus and polyinosinic:polycytidylic acid, poly(I:C), treatment (fig. S5). Importantly, we reproduced the inhibitory effect of CPT and TPT on PAMP-induced gene expression using a different cell line, the murine macrophage RAW 264.7 (fig. S6A). Of note, Top1 inhibition does not suppress the response to other stimuli such as estrogen signaling and heat shock, as indicated by the analysis of prototypical target genes (fig. S7, A and B, respectively).

Furthermore, chemical inhibition and loss-of-function experiments in A549 cells indicate that class II Topoisomerase enzymes (Top2) do not fully phenocopy Top1 activity during PAMP-responsive gene induction (fig. S8), and along with previous observations (*29*, *35*, *36*), suggest that inhibition of topoisomerases can elicit cell type- and gene-specific effects. Notably, and in line with what others have recently shown (*29*), neither TPT- nor CPT-treated cells displayed DNA damage at the concentration we used (fig. S9).

We then characterized the genomic distribution of RNAPII and Top1 during infection, in the presence and absence of Top1 inhibition. Our results show reduced promoter levels of RNAPII and Top1 at PAMP-induced genes in infected A549 cells (Fig. 2B) and macrophages (fig. S6B) when Top1 is inhibited. Notably, RNAPII and Top1 levels at housekeeping genes are not reduced as a result of Top1 inhibition (Fig. 2B and fig. S6B), consistent with their unaffected gene expression (Fig. 2A and fig. S6A). Reduced RNAPII targeting at PAMP-induced loci was confirmed by ChIP-sequencing (Fig. 2C) and by the analysis of the RNAPII tracks at representative PAMP-induced genes and housekeeping genes (Fig. 2D).

To link cause (Top1 inhibition) and effect (RNAPII levels at promoters), we devised a strategy to map the genomic distribution of Top1 inhibitors via chem-ChIP, a method used to reveal the genomic localization of drugs (*37*). In brief, we first 'in house' synthesized an analog of TPT (we did not succeed with CPT), which is amenable for coupling with a derivative of biotin. This compound was called TPT alkyne [(TPT-A; Fig. 2E)]. TPT-A synthesis and experimental strategy are shown in fig. S10, A and B; the validation that TPT-A is as effective as TPT is shown in fig. S10, C and D. We then performed Chem-ChIP and analyzed the distribution of TPT-A on chromatin. At basal state, TPT-A was enriched at promoters and gene bodies of active genes like ACTB and HPRT genes (Fig. 2F) as expected based on the fact that Top-1 travels with elongating RNAPII and supported by the genome-wide distribution of Top1 (*31*, *38*).

During infection, TPT-A distribution peaks at promoters of inducible genes IFIT1 and IFIT2 (Fig. 2F) but not into gene bodies, suggesting that the presence of the inhibitor does not allow RNAPII and Top1 into productive transcriptional cycles. Indeed, TPT-A distribution is inversely correlated with RNAPII and Top1 density only at promoters of PAMP-induced genes (Fig. 2B).This indicates that TPT-A suppression of Top1 activity leads to a specific inhibition of RNAPII targeting at most PAMP-responsive *loci* (Fig. 2C). These results i) corroborate the absence of an effect of Top1 inhibition at housekeepers, ii) indicate that such genes can escape the transcriptional consequences of Top1 inhibition (likely via Top2, fig. S8D), and iii) designate a RNAPII activator-like function for Top1 at PAMP-induced loci.

Top1 facilitates expression of genes that require nucleosome remodeling for activation

Previous work has characterized how, based on genetic and epigenetic features, classes of inducible genes respond temporally to Toll like receptor (TLR; a class of PRRs) induction (*39–42*). These studies provide a framework to address the specificity of Top1's effect during viral PAMP stimulation.

We first selected the Top1-affected genes whose expression was upregulated more than two fold upon infection (Fig. 3 and table S1). Similarly to (*40*), we then characterized this gene set based on the dependency on the interferon regulatory factor 3 (IRF3) and the SWItch/Sucrose Non-Fermenter (SWI/SNF)-nucleosome remodeling complex for transcriptional activation. To do so, we performed RNAi-mediated depletion of the two catalytic subunits of the SWI/SNF complex, SMARCA2 and SMARCA4, prior to and after infection with influenza virus or IFN-treatment (Fig. 3A). This resulted in 4 distinct classes of Top1-affected genes, as depicted in Fig. 3B.

Strikingly, the vast majority of genes controlled by Top1 are dependent on SWI-SNF nucleosome remodeling (75% genes). At basal state, these genes (compared to SWI-SNF independent genes and housekeeping genes) are almost devoid of TATA-binding protein (TBP) and RNAPII and display high levels of histone H3 at their promoters (Fig. 4A). These features indicate that nucleosome remodeling at these genes precedes recruitment of RNAPII and transcriptional initiation. Upon infection, Top1-affected genes are linked to transcriptional induction (as measured by histone H4 acetylation; fig. S11) and to broad expression levels, as measured by RNAPII recruitment (Fig. 4A) and expression data (inset

Fig. 4A). Inhibition of Top1 leads to diminished RNAPII and TBP with a concomitant re-integration of H3 at promoters (Fig. 4A).

Genes which require remodeling for their activation are dependent on co-activators (*42*) and possess unique chromatin features at basal state, namely: low levels of active histone marks, low levels of preloaded RNAPII, low CpG island content (*40*). All these identifying features were recapitulated in Top1-affected genes by using genome wide analyses and mathematical modeling of public datasets (Fig. 4B-D, fig. S12, and table S3).

Top1 inhibition suppresses the response to bacterial stimuli and pro-inflammatory cytokines

To understand whether Top1 is required to activate the expression of pro-inflammatory genes induced by stimuli other than viruses, we characterized the effect of Top1 inhibition after exposure to bacterial PAMPs and exogenous cytokines. First, we treated both epithelial and macrophage cell lines with the bacterial-PAMP lipopolysaccharide (LPS). Top1 inhibition suppressed the expression of anti-microbial genes, as indicated by the transcriptional analysis of representative pro-inflammatory cytokines (Fig. 5, A and B). Accordingly, Top1 inhibition resulted in reduced levels of Top1 and RNAPII at promoters of the affected genes (fig. S13, A and B).

The expression of anti-microbial genes upon PRR stimulation induces the secretion of pro-inflammatory signals, which trigger the maturation and activation of other innate immune cells expressing the corresponding receptors (*43*). To further extend our findings on cells activated via stimulation by inflammatory cytokines, we incubated both A549 and RAW cells with exogenous IFN-β and tumor necrosis factor-α (TNFα). We then monitored gene expression changes, as well as promoter levels of RNAPII and Top1, in untreated and Top1-inhibited cells. As shown by the expression of multiple target genes (fig. S14, A and B) and respective chromatin occupancies (fig. S14, C and D), repression of Top1 activity inhibited IFN-β- and TNFα-induced gene expression in both cell types analyzed, paralleling our results using viral and bacterial stimuli.

Top1 protects against lethal inflammation in vivo

Altogether, our data suggested that Top1 inhibition could be an effective way to suppress the exacerbated response to pathogenic stimuli, and prompted us to characterize the role of Top1 inhibition in vivo. We first analyzed whether in vivo preventive inhibition of Top1 activity rescued animals from lethal endotoxic shock. This was indeed the case, where 90% of animals pretreated with CPT were rescued (Fig. 5C). The protective effect of Top1 inhibition in vivo is not caused by cellular damage (Fig. 5, F to H) but by suppressing inflammatory cytokines (Fig. 5, D and E).

In order to test the potential of Top1 inhibition therapy in a model of bacterial disease, we infected mice with *Staphyloccocus aureus* (*S. aureus*), which is one of the predominant pathogens causing nosocomial infections and sepsis in humans (*44*). Our results indicate that therapeutic treatment with CPT allowed 70% of the mice to survive the lethal challenge (Fig. 6A). Since the inflammatory response against Influenza is believed to be responsible for the enhanced susceptibility to pneumonia after secondary infection with *S. aureus* in both mice and humans (*45*), we also tested whether CPT treatment could reverse the outcome of viral bacterial co-infection. For this, mice inoculated with the influenza virus PR8 (H1N1 PR8 A/Puerto Rico/8/1934 strain) were treated with CPT at 12, 24 and 36 hours post-infection. Three days after viral infection, mice received a challenge with *S. aureus*. As shown in Fig. 6B, CPT treatment rescues 94% of the animals from the lethal co-infection challenge without impairing the differentiation of virus-specific CD8 T cells into IFN-γ/TNFα-producing effector cells (fig. S15). Strikingly, a similar protective effect (90% rescue of mortality) was also present when therapeutically inhibiting Top1 in an endotoxin-induced mouse model of acute liver-failure, where the pathology is caused by high levels of cytokine secretion such as TNFα (Fig. 6C) (*46*). These data suggest that, in experimental models of lethal-inflammation, therapeutic Top1 inhibition provides meaningful protection at the organismal level.

Finally, since an elevated mortality rate associated with an exacerbated pro-inflammatory response and clinical symptoms similar to septic shock is also observed in humans after infection with highly pathogenic viruses, we focused on *Zaire ebolavirus* (Ebola virus), which recently caused a large outbreak of illness with a high fatality rate in West Africa (*47*). We profiled the global gene expression response during Ebola (*WT* strain Zaire-Mayinga) infection in the human leukemic cell line THP-1, in the presence and absence of Top1 inhibition. Our analysis shows that Ebola virus-induced genes IL-8, IL-1B and TNF are suppressed by Top1 inhibition (Fig. 7 and table S4). Overall, these data highlight a protective role for Top1 inhibition during infections both in vitro and in vivo.

Discussion

Topoisomerase activities are required at all genes in order to resolve topological constrains that result from RNAPII activity. Recent works (*29*, *30*) have shown that short and reversible Top1 inhibition specifically suppresses the expression of long genes. This indicated a differential susceptibility of genes to Top1 inhibition and redundant Top1 activities at the promoters of housekeepers. Here, we report the surprising evidence that during infection, short

and reversible inhibition of Top1, as well as Top1 depletion, specifically suppresses genes induced by microbial agents. Our study reveals a gene specific activator-like role for Top1. Concordantly, such an effect was shown using in vitro transcriptional assays (*32*, *33*). The consequence of Top1 inhibition during infection is a suppression of RNAPII recruitment at PAMP-induced promoters. This effect is more prominent at genes with a bigger difference in the levels of RNAPII at basal and induced states, which explains why compromising Top1 function affects inducibility of PAMP-responsive genes. The specificity of Top1 inhibition is then geared toward genes that are not prone to immediate activation but require co-activator (IRF3) assisted nucleosome remodeling. Other co-transcriptional events, along RNA stability or transport, are likely to contribute to PAMP-gene suppression by Top1 inhibition.

At the mechanistic level, Top-1 inhibitors may create a local chromatin environment that is non-permissive to transcription, or alternatively, could titrate out new recruitment of Top1. Both scenarios would lead to defects in RNAPII recycling and re-initiation and cause the observed suppressive effect at pathogen-induced genes. Since Top1 facilitates the expression of inflammatory genes, Top1 depletion or chemical inhibition during infection reduces the immune response associated with microbial recognition. This effect was evident in vitro by chemical inhibition of Top1 causing suppression of both virus- and inflammatory signal- induced host gene expression, and in vivo by displaying protective effects in mouse models of lethal inflammation. The cellular response against microbes is essential in protecting us against infection, but its hyper-activation can have fatal consequences. Our results suggest that a Top1 inhibition therapy could be useful in many instances, such as in pandemics and many congenital deficiencies, whereby an overt immune response is acutely induced.

Materials and methods

Cell lines and viruses

The following cell lines were originally obtained from the American Type Culture Collection (ATCC): A549 cells (adenocarcinomic human alveolar basal epithelial cells), 293T cells (human embryonic kidney cells), RAW 264.7 cells (mouse leukemic monocyte macrophage cell line), and HTBE cells (human primary bronchial/tracheal epithelial cells).

The 293T-FF cell line was generated by transfection with the plasmid pGL4.17-IFN-FF, encoding a cassette with the firefly luciferase gene under the control of the murine IFN-β promoter, as previously described (*48*), and was a kind gift from P. Palese.

Cells were maintained in culture at 37°C with 5% CO_2 in Dulbecco's minimal essential medium (DMEM, Gibco, Life Technologies) supplemented with 2 mM glutamine (Life Technologies), 10% FBS (Hyclone), 100 U/mL penicillin (Life technologies) and 100 μg/mL streptomycin (Gibco, Life Technologies).

The influenza virus PR8ΔNS1, which is the H1N1 PR8 A/Puerto Rico/8/1934 strain lacking the expression of the NS1 protein, was propagated in MDCK cells expressing the viral nonstructural protein 1 (NS1) (*49*). The influenza virus PR8 expressing the green fluorescent protein (GFP) (PR8-GFP) and deficient for the viral protein hemagglutinin (HA), was propagated in MDCK-HA-expressing cells (*50*). Both PR8ΔNS1 and PR8-GFP viruses as well as the MDCK cells were kind gifts from A. García-Sastre.

The influenza virus H3N2, which is the strain A/Philippines/2/82, was propagated in 10-day-old embryonated chicken eggs and was a kind gift from F. Kramer.

The Sendai virus (SeV), Cantell strain, was propagated in 10-day old embryonated chicken eggs (*51*), and was a kind gift from P. Palese.

Viral infections using the strains described above were performed at a multiplicity of infection (MOI) of 3 and cells were analyzed at different time points as indicated in the figures.

Infections with the Ebola virus were performed in THP-1 cells, a human monocytic cell line that naturally expresses several Pattern Recognition Receptors. We used the *wild-type* Ebola Zaire-Mayinga strain and its VP-35 mutant, which fails to block the type I Interferon response in the host (*52*). Cells were recovered 24 hours after Ebola infection.

IRF3 dependent genes were compiled from the literature and cross-compared with a list of genes induced by IRF3-5D in $STAT1^{-/-}$ cells (courtesy of S. Tripathi).

Cell viability assay

The Cell Titer Glo Cell Viability Assay (Promega) detects adenosine triphosphate (ATP) levels as a function of cell viability, and was used according to manufacturer's specifications. Briefly, cells were seeded into 96-well plates (5000 cells/well), and eighteen hours later, 25 μL of fresh media containing the indicated compounds (serially diluted) were included. After 6 hours of incubation, 50 μL of CellTiterGlo was added and the luminescence was measured. Vehicle treated cells were used to normalize (100%) the ATP activity.

The CytoTox 96 Non-Radioactive Cytotoxicity Assay (Promega), a colorimetric assay measuring the release of the cellular enzyme lactate dehydrogenase (LDH), was also used according to manufacturer's specifications.

Inhibitors and cell treatments

Cell culture: Camptothecin (CPT, Sigma) was dissolved in a 4:1 mixture of chloroform:methanol at the concentration

of 0.5 mM, heated at 55°C until fully dissolved and then added to cells in DMEM medium at the final concentration of 0.5 μM. Topotecan (TPT, Sigma) and TPT-Alkyne (TPT-A) were dissolved in dimethyl sulfoxide (DMSO, Fisher) at the concentration of 100 μM and then added to cells in DMEM medium at the final concentration of 100 nM. Flavopiridol and (+/−)-JQ1 (both from Sigma) were dissolved in DMSO at the concentration of 0.5 mM and then added to cells in DMEM medium at the final concentration of 0.5 μM. Doxorubicin (DOXO, Sigma) was dissolved in water at the concentration of 50 μM and then added to cells in DMEM medium at the final concentrations of 0.5 and 5 μM.

All the compounds and the vehicle control DMSO were added to the cell cultures at one hour before and after stimulation or infection.

Lipopolysaccharide (LPS, Sigma, tlrl-3pelps) was added to cells in DMEM medium at the final concentration of 100 ng/mL for 2 hours. Tumor necrosis factor alpha (TNFα, Sigma, human: T0157, mouse: T7539), Interferon-β (IFN-β, PBL Assay Science, human: 11415-1, mouse: 12400-1), and polyinosinic-polycytidylic acid (poly(I:C), Sigma, P1530) were added to cells in DMEM medium for 4 hours at the final concentration of 10 ng/mL, 100 U/mL, and 10 μg/mL, respectively.

For hormone treatment, A549 cells were grown in DMEM containing 5% charcoal-dextran–treated FBS (Sigma) for 2 days before addition of 10 nmol/L 17β-estradiol (Sigma, E2758).

For heat shock, A549 cells were incubated at 42°C for 2 hours.

In vivo experiments: CPT was dissolved in a 4:1 mixture of chloroform:methanol, followed by heating at 55°C until fully dissolved. CPT was then brought up with water to the necessary volume corresponding to 200 μl/mouse and centrifuged for 5 min at 4,000 rpm. The top aqueous fraction, containing the CPT, was recovered and dissolved at the final concentration of 30 mg/kg of mouse weight in 200 μl of water for each injection.

Immunofluorescence

A549 and RAW 264.7 cells were cultured on coverslips overnight and then treated with 0.5 and 10 μM of CPT or 100 nM and 10 μM of TPT one hour before and post-infection (p.i.) with PR8ΔNS1 or H3N2 viruses. At 6 hours p.i., cells were fixed for 10 min at 4°C in 4% formaldehyde (EMS). Coverslips were washed in PBS (Life Technologies) and cells were permeabilized for 10 min at room temperature in 0.5% NP-40 (Sigma). Coverslips were washed again in PBS and nonspecific binding was blocked by incubation for 30 min at room temperature with a solution containing 3% BSA (Sigma) in PBS. Cells were then probed for 2 hours with a rabbit anti-phospho-histone H2A.X antibody (Cell Signaling), followed by detection with Alexa Fluor 488-conjugated (green) goat anti-rabbit IgG (heavy and light chain, Life Technologies). DNA was counterstained with 4,6-diamidino-2-phenylindole (DAPI, Thermo Scientific).

For visualization of the PR8-GFP virus, an EVOS FL (Thermo Scientific) microscope was used.

Quantitative PCR

For RNA extraction, cells were homogenized with QI-Ashredder columns (Qiagen). RNA was extracted using the RNeasy Mini Kit and then treated with the RNase free DNase kit (all Qiagen). Proteins were also simultaneously recovered from cell lysates by acetone precipitation of the flow-through from RNeasy spin columns, according to manufacturer's instructions.

cDNA was in vitro transcribed using a High-Capacity cDNA RT Kit (Thermo Fisher Scientific) or a SuperScript III First-Strand Synthesis SuperMix (Life Technologies). Quantitative PCR (qPCR) was performed using the iTaq Universal SYBR® Green One-Step Kit (Bio-Rad), according to manufacturer's instructions.

The statistical significance of all pairwise comparisons in qPCR assays' change in cycling threshold (ΔC_T) values was determined with a two-tailed Student's *t*-test under the assumption of equal variances between groups. We did not find significant differences (false-discovery rate, $q < 0.05$) between contrast groups in Levene's tests of equality of variances, or departures from normality as assessed by Shapiro-Wilk tests.

Primers

Primers were designed using the Primer3 online-tool or by using already available primers from Harvard's PrimerBank database.

Sequences of primers used for qPCR were as follows:

Human. β-actin forward, 5′-ACCTTCTACAATGAGCTGCG-3′, and β-actin reverse, 5′-CCTGGATAGCAACGTACATGG-3′; GAPDH forward, 5′-GCAAATTCCATGGCACCGT-3′, and GAPDH reverse, 5′-GCCCCACTTGATTTTGGAGG-3′; 18S forward, 5′-GTAACCCGTTGAACCCCATT-3′, and 18S reverse, 5′-CCATCCAATCGGTAGTAGCG-3′; IFIT2 forward, 5′-AGGCTTTGCATGTCTTGG-3′, and IFIT2 reverse, 5′GAGTCTTCATCTGCTTGTTGC-3′; IFIT1 forward, 5′-TTCGGAGAAAGGCATTAGA, and IFIT1 reverse, 5′-TCCAGGGCTTCATTCATAT; IFNB1 forward, 5′-TCTGGCACAACAGGTAGTAGGC, and IFNB1 reverse, 5′-GAGAAGCACAACAGGAGAGCAA; HPRT1 forward, 5′-GAAAAGGACCCCACGAAGTGT, and HPRT1 reverse, 5′-AGTCAAGGGCATATCCTACAACA; BRD4 forward, 5′-GAGCTACCCACAGAAGAAACC, and BRD4 reverse, 5′-GAGTCGATGCTTGAGTTGTGTT; IL-1β forward, 5′-

ATGATGGCTTATTACAGTGGCAA, and IL-1β reverse, 5′-GTCGGAGATTCGTAGCTGGA; IL-6 forward, 5′-ACTCACCTCTTCAGAACGAATTG, and IL-6 reverse, 5′-CCATCTTTGGAAGGTTCAGGTTG; IL-8 forward, 5′-TTTTGCCAAGGAGTGCTAAAGA, and IL-8 reverse, 5′-AACCCTCTGCACCCAGTTTTC; CDK9 forward, 5′-ATGGCAAAGCAGTACGACTCG, and CDK9 reverse, 5′-GCAAGGCTGTAATGGGGAAC; CCNT1 forward, 5′-ACAACAAACGGTGGTATTTCACT, and CCNT1 reverse, 5′-CCTGCTGGCGATAAGAAAGTT; CXCL10 forward, 5′-GTGGCATTCAAGGAGTACCTC-3′, and CXCL10 reverse, 5′-TGATGGCCTTCGATTCTGGATT-3′; IFIT3 forward, 5′-AGAAAAGGTGACCTAGACAAAGC-3′, and IFIT3 reverse, 5′-CCTTGTAGCAGCACCCAATCT-3′; ZFP36 forward, 5′-GAGAACAAATTCCGGGACCG-3′, and ZFP36 reverse, 5′-GCGTGGAGTTGATCTGGGAG-3′; CCL5 forward, 5′-CCAGCAGTCGTCTTTGTCAC-3′, and CCL5 reverse, 5′-CTCTGGGTTGGCACACACTT-3′; GBP1 forward, 5′-AACGACAGGGTCCAGTTGCTGAAAG, and GBP1 reverse, 5′-TAGGGGTGACAGGAAGGCTCTGG; OASL forward, 5′-CTGATGCAGGAACTGTATAGCAC, and OASL reverse, 5′-CACAGCGTCTAGCACCTCTT; IFIH1 forward, 5′-TCACAAGTTGATGGTCCTCAAGT, and IFIH1 reverse, 5′-CTGATGAGTTATTCTCCATGCCC; IFI6 forward, 5′-GGTCTGCGATCCTGAATGGG, and IFI6 reverse, 5′-TCACTATCGAGATACTTGTGGGT; OAS2 forward, 5′-ACGTGACATCCTCGATAAAACTG, and OAS2 reverse, 5′-GAACCCATCAAGGGACTTCTG; SPRY2 forward, 5′-CCTACTGTCGTCCCAAGACCT, and SPRY2 reverse, 5′-GGGGCTCGTGCAGAAGAAT; DDX58 forward, 5′-TGCGAATCAGATCCCAGTGTA, and DDX58 reverse, 5′-TGCCTGTAACTCTATACCCATGT; RSAD2 forward, 5′-TTGGACATTCTCGCTATCTCCT, and RSAD2 reverse, 5′-AGTGCTTTGATCTGTTCCGTC; TRIM22 forward, 5′-AATGTGCTGGATAACCTGGCA, and TRIM22 reverse, 5′-TCTACTGACGATCCCCTCAAC; ISG15 forward, 5′-CGCAGATCACCCAGAAGATCG, and ISG15 reverse, 5′-TTCGTCGCATTTGTCCACCA; UBE2L6 forward, 5′-TGGACGAGAACGGACAGATTT, and UBE2L6 reverse, 5′-GGCTCCCTGATATTCGGTCTATT; TRIM21 forward, 5′-TCAGAGCTAGATCGAAGGTGC, and TRIM21 reverse, 5′-ACTCACTCCTTTCCAGGACAAT; IFITM1 forward, 5′-GGGCCTTCTGGATTCCGAG, and IFITM1 reverse, 5′-CGTGGGGTTGGTCATCGTC; HERC5 forward, 5′-GGTGAGCTTTTTGCCTGGG, and HERC5 reverse, 5′-TTCTCCGGCAGAAATCTGAGC; CDKN2C forward, 5′-GGGGACCTAGAGCAACTTACT, and CDKN2C reverse, 5′-CAGCGCAGTCCTTCCAAAT; ISG20 forward, 5′-TCTACGACACGTCCACTGACA, and ISG20 reverse, 5′-CTGTTCTGGATGCTCTTGTGC; ZC3HAV1 forward, 5′-TCACGAACTCTCTGGACTGAA-3′, and ZC3HAV1 reverse, 5′-ACTTTTGCATATCTCGGGCATAA-3′; JUN forward, 5′-ATCAAGGCGGAGAGGAAGCG-3′, and JUN reverse, 5′-TGAGCATGTTGGCCGTGGAC -3′; BAMBI forward, 5′-ATGCTCTCCCGTTTGCACTAC-3′, and BAMBI reverse, 5′-AGGATCTTATCGTTGCTGAGGT-3′; MX2 forward, 5′-CAGAGGCAGCGGAATCGTAA-3′, and MX2 reverse, 5′-TGAAGCTCTAGCTCGGTGTTC-3′; IFI44 forward, 5′-GGTGGGCACTAATACAACTGG, and IFI44 reverse, 5′-CACACAGAATAAACGGCAGGTA; TNF-alpha forward, 5′-CCTCTCTCTAATCAGCCCTCTG, and TNF-alpha reverse, 5′-GAGGACCTGGGAGTAGATGAG; GFP forward, 5′-AAGCTGACCCTGAAGTTCATCTGC, and GFP reverse, 5′-CTTGTAGTTGCCGTCGTCCTTGAA; PR8 HA forward, 5′-AAAGAAAGCTCATGGCCCAACC, and PR8 HA reverse, 5′-TCCTTCTCCGTCAGCCATAGCA; PR8 PB1 forward, 5′-TCATGAAGGGATTCAAGCCG, and PR8 PB1 reverse, 5′-GGAAGCTCCATGCTGAAATTG; HSP70 forward, 5′-CATCGCCTATGGGCTGGAC, and HSP70 reverse, 5′-GGAGAGAACCGACACATCGAA; HSP27 forward, 5′-ACGGTCAAGACCAAGGATGG, and HSP27 reverse, 5′-AGCGTGTATTTCCGCGTGA; PGR1 forward, 5′-TCCACCCCGGTCGCTGTAGG, and PGR1 reverse, 5′-TAGAGCGGGCGGCTGGAAGT; TFF1 forward, 5′-TTGGAGAAGGAAGCTGGATGG, and TFF1 reverse, 5′-ACCACAATTCTGTCTTTCACGG; GREB1 forward, 5′-GTGGTAGCCGAGTGGACAAT, and GREB1 reverse, 5′-ATTTGTTTCCAGCCCTCCTT; TOP1 forward, 5′-AAGGTCCAGTATTTGCCCCAC, and TOP1 reverse, 5′-ATTCATGGTCGAGCATTTTTGC; TOP2A forward, 5′-ACCATTGCAGCCTGTAAATGA, and TOP2A reverse, 5′-GGGCGGAGCAAAATATGTTCC; TOP2B forward, 5′-TTGGACAGCTTTTAACATCCAGT, and TOP2B reverse, 5′-GCACCATAACCATTACGACCAC; SMARCA2 forward, 5′-AGGGGATTGTAGAAGACATCCA, and SMARCA2 reverse, 5′-TTGGCTGTGTTGATCCATTGG; SMARCA4 forward, 5′-AATGCCAAGCAAGATGTCGAT, and SMARCA4 reverse, 5′-GTTTGAGGACACCATTGACCATA.

Mouse. *Actb* forward, 5′-TTACGGATGTCAACGTCACAGTTC, and *Actb* reverse, 5′-ACTATTGGCAACGAGCGGTTC; *Mip1a* forward, 5′-CGAGTACCAGTCCCTTTTCTGTTC, and *Mip1a* reverse, 5′-AAGACTTGGTTGCAGAGTGTCATG; *Il-6* forward, 5′-TGAGATCTACTCGGCAAACCTAGTG, and *Il-6* reverse, 5′-CTTCGTAGAGAACAACATAAGTCAGATACC; *Ifit1* forward, 5′-GCCTATCGCCAAGATTTAGATGA, and *Ifit1* reverse, 5′-TTCTGGATTTAACCGGACAGC; *Ifit2* forward, 5′-AGAACCAAAACGAGAGAGAGTGAGG, and *Ifit2* reverse, 5′-TCCAGACGGTAGTTCGCAATG; *Mip-2* forward, 5′-GTCCCTCAACGGAAGAACCAA, and *Mip-2* reverse, 5′-ACTCTCAGACAGCGAGGCACAT; *Rantes* forward, 5′-TGCCCACGTCAAGGAGTATTTC, and *Rantes* reverse, 5′-TCCTAGCTCATCTCCAAATAGTTGATG; *Il-1β* forward, 5′-GCAACTGTTCCTGAACTCAACT, and *Il-1β* reverse, 5′-

ATCTTTTGGGGTCCGTCAACT.

Sequences of primers used for ChIP followed by qPCR were as follows:

Human. ACTB *5′* forward, GAGGGGAGAGGGGGTAAAA, and ACTB *5′* reverse, AGCCATAAAAGGCAACTTTCG; IFIT1 *5′* forward, AGAGGAGCCTGGCTAAGCA, and IFIT1 *5′* reverse, GGTTGCTGTAAATTAGGCAGC; IFIT2 *5′* forward, TGCACTGCAACCATGAGG, and IFIT2 *5′* reverse, TGACTCAACAGCACTACCGA; IL-6 *5′* forward, CCCAATAAATATAGGACTGGAGATG, and IL-6 *5′* reverse, GAGTTCATAGCTGGGCTCCT; IL-8 *5′* forward, TATAAAAAGCCACCGGAGCA, and IL-8 *5′* reverse, GCCAGCTTGGAAGTCATGTT; CXCL10 *5′* forward, CAGCAGAGGAACCTCCAGTC, and CXCL10 *5′* reverse, TGATGTTCCTTACCTTGAATGC; IFIT3 *5′* forward, CGGAACAGCAGAGACACAGA, and IFIT3 *5′* reverse, GGGAAAAACCCCTCAAACAT; ZFP36 *5′* forward, ACTTCAGCGCTCCCACTCT, and ZFP36 *5′* reverse, AGTTGGAGAAGGGAGGCAAG; CCL5 *5′* forward, CGAATTTCCGGAGGCTATTT, and CCL5 *5′* reverse, CGTGCTGTCTTGATCCTCTG; GBP1 *5′* forward, ATGAGGAAATCCCAGCCCTA, and GBP1 *5′* reverse, TCCTTAGTTCACGAGCACTGG. OASL *5′* forward, AAATGCTCCTGCCTCAGAAA, and OASL *5′* reverse, GGGACAGAGATGGCACTGAT; IFIH1 *5′* forward, GAAGGAGGTTCAGCAGTTGG, and IFIH1 *5′* reverse, AGCACCTTGGAGAAGGGAGT; IFI6 *5′* forward, TGATGCCCACACTTCATAGC, and IFI6 *5′* reverse, GGGAGGATCCACAAGTGATG; OAS2 *5′* forward, TTTCAGTTTCCTGGCTCTGG, and OAS2 *5′* reverse, TGGATAAACCAACCCAGCTT; SPRY2 *5′* forward, AAAGAGAATTCGGAGCCAGA, and SPRY2 *5′* reverse, ATCTGCCAGGAAAAGGGACT; DDX58 *5′* forward, CCTTTCACCTCTTTCCCAGA, and DDX58 *5′* reverse, CTTTTCCAGACCGAATAGCTT; RSAD2 *5′* forward, CCAATGACAGGTTGCTCAGA, and RSAD2 *5′* reverse, CAGCTGCTGCTTTCTCCTCT; TRIM22 *5′* forward, CTGAGTGCCTTGCCAGTACA, and TRIM22 *5′* reverse, CAAATGAGTTTCCCCACAGG; ISG15 *5′* forward, GCTGAGAGGCAGCGAACTC, and ISG15 *5′* reverse, CCCCACCTGTGACATCTGC; UBE2L6 *5′* forward, CCGGGACTCACGGTCTTT, and UBE2L6 *5′* reverse, CGGAGCGAAGACTGGAAC; TRIM21 *5′* forward, GCTCAAGGATGGAGACTGGA, and TRIM21 *5′* reverse, CCTCCCCTTTCCTCTCAGAC; IFITM1 *5′* forward, AACTGAAACGACAGGGGAAA, and IFITM1 *5′* reverse, ACAGCCACCTCATGTTCCTC; HERC5 *5′* forward, ACCAGGCGTTCTCTCCTCTC, and HERC5 *5′* reverse, CTGGGAAAGAGCCAGAGC; IFNB1 *5′* forward, GGAATCCAAGCAAGTTGTAGC, and IFNB1 *5′* reverse, AACCTTTCGAAGCCTTTGCT; CDKN2C *5′* forward, GCCGAGCCTCCTTAAAACTC, and CDKN2C *5′* reverse, ACAATTGCTGCTTCTGTTGC; ISG20 *5′* forward, GGTAGCCCAGGAGATGGAG, and ISG20 *5′* reverse, CTCACGTCTGCCTCTCTGCT; Z3HAV1 *5′* forward, CGCATCTGCATTTAGACGAA, and ZC3HAV1 *5′* reverse, CTCAACAGGGCTCTCAGGAC; JUN *5′* forward, CCGTTGCTGGACTGGATTAT, and JUN *5′* reverse, CCCCAAGATCCTGAAACAGA; BAMBI *5′* forward, CGTGCTGTGGAGACCCTACT, and BAMBI *5′* reverse, CCAGGAGCCCAGAAAAGTT; MX2 *5′* forward, CCACAGCTCTCCCAGGATT, and MX2 *5′* reverse, TGTGGCATATGAACCACTCC; IFI44 *5′* forward, TGAGAGAAGTTGGCATGCTG, and IFI44 *5′* reverse, AGCTGAGGGTAGCTGCTCTGT; IRF1 *5′* forward, AAGAGGGAAGAAGGCAGAGG, and IRF1 *5′* reverse, CTTAGTCGAGGCAAGACGTG; KLF4 *5′* forward, TCTCTCTGGTCGGGAAACTG, and KLF4 *5′* reverse, GCGCCGAGTTTGTTGATTTA; GAPDH *5′* forward, ACAGTCAGCCGCATCTTCTT, and GAPDH *5′* reverse, TTCTCTCCGCCCGTCTTC.

Mouse. *Actb* *5′* forward, GGGCTACAGTGGGTGAAAGG, and *Actb* *5′* reverse, GGGCTACAGTGGGTGAAAGG; *Ifit1* *5′* forward, TGAAAAGAGCACACCCCCTA, and *Ifit1* *5′* reverse, CTCCTCAGAAACCTGCCTTG; *Ifit2* *5′* forward, AGCCACACCCGACTAACG, and *Ifit2* *5′* reverse, CTTGGTGCTTTGAGGGATCT; *Il-6* *5′* forward, AATGTGGGATTTTCCCATGA, and *Il-6* *5′* reverse, GCGGTTTCTGGAATTGACTATC; *Mip2-a* *5′* forward, GGGCTTTTCCAGACATCGT, and *Mip2-a* *5′* reverse, TGAAGTGTGGCTGGAGTCTG.

Sequences of primers used for Chem-ChIP followed by qPCR were as follows:

Human. ACTB upstream forward, CTGCAGAAGGAGCTCTTGGA, and ACTB upstream reverse, GACCCACCCAGCACATTTAG; ACTB-1 forward, GAGGGGAGAGGGGGTAAAA, and ACTB-1 reverse, AGCCATAAAAGGCAACTTTCG; ACTB-2 forward, GTCATCTTCTCGCGGTTGG, and ACTB-2 reverse, GGCATCCTCACCCTGAAGTA; ACTB-3 forward, CCTACACCCACAACACTGTCT, and ACTB-3 reverse, TGACCTGAGTCTCCTTTGGAA; ACTB-4 reverse, CAGGTCCAGACGCAGGAT, and ACTB-4 reverse, GCCATGTACGTTGCTATCCA; ACTB-5 forward, GTGCCAGGGCAGTGATCT, and ACTB-5 reverse, CTGTGGCATCCACGAAACTA; ACTB-6 forward, CTAAGTCATAGTCCGCCTAGAAGC, and ACTB-6 reverse CTGTCCACCTTCCAGCAGAT; ACTB downstream forward, CGCCCAGTCTCCAGTCAC, and ACTB downstream reverse, GTTGGGGTAGGGGGTCCA; HPRT1 upstream forward, TAGTCGGGGTTCTCCACAAA, and HPRT1 upstream reverse, CCTTCAGATTTTGGACTCAACA; HPRT1-1 forward, GAAAATTCCCACGGCTACCT, and HPRT1-1 reverse,

GGGAAAGCCGAGAGGTTC; HPRT1-2 forward, GACAGAGTCTTGCTCTGTTTCC, and HPRT1-2 reverse, AAAATTAGCCGGGTGTGGT; HPRT1-3 forward, GCCTGGGCTAGACTTTTGAG, and HPRT1-3 reverse, TGACAGGTGTCTGGTTCTGG; HPRT1-4 forward, CTGGACCTCCTGGAATTGAG, and HPRT1-4 reverse, AAACACAGGTAGAACTATAAAAGCAAA; HPRT1-5 forward, GATGCTCACCTCTCCCACAC, and HPRT1-5 reverse, CCCTGACTACCCATGTGTCC; HPRT1-6 forward, TGTCATTAGTGAAACTGGAAAAGC, and HPRT1-6 reverse, CATGCAAAAAGCTCTACTAAGCA; HPRT1 downstream forward, CGTCTGGGGTCATACAGGTT, and HPRT1 downstream reverse, CTGAGGGCAGGGATAGTTTG; IFIT1 upstream forward, CAAGACTGCTGCCAAATTCA, and IFIT1 upstream reverse, CATGATCAGGCCATAAGCAA; IFIT1-1 forward, AGAGGAGCCTGGCTAAGCA, and IFIT1-1 reverse, GGTTGCTGTAAATTAGGCAGC; IFIT1-2 forward, AACAGGTTTTCGCAATCAGG, and IFIT1-2 reverse, CTTCCCAAGCAGATGTGGAT; IFIT1-3 forward, AACATTTTTCTCGCTATGTGGA, and IFIT1-3 reverse, GACAGAAAGCAGATTAACAGTTGC; IFIT1-4 forward, TTTTCATGGCTGTCATCAGATT, and IFIT1-4 reverse, TTCCACTCAGATTGGCAAGA; IFIT1-5 forward, ACTATTTGAGATCCCTTGACATTT, and IFIT1-5 reverse, GATGTCAATACTACCCAAAGTGATCT; IFIT1-6 forward, GAAATATGAATGAAGCCCTGGA, and IFIT1-6 reverse, GGCTGATATCTGGGTGCCTA; IFIT1 downstream forward, AGCTGCAGCCTGAGAGTTTG, and IFIT1 downstream reverse, CCAGTCCCCATGATCTGAGT; IFIT2 upstream forward, GAGGACTTTAAATGATACCAACACA, and IFIT2 upstream reverse, TTTCCCCCTTTTTATTGATGT; IFIT2-1 forward, TGCACTGCAACCATGAGG, and IFIT2 5′ reverse, TGACTCAACAGCACTACCGA; IFIT2-2 forward, TCAGAGAAAGAAGGCAGCAGA, and IFIT2-2 reverse, AAGACAGGGTCAGTGCACAA; IFIT2-3 forward, AACCCAAAATCAAGCAGTGAA, and IFIT2-3 reverse, TGTGCATTTGCAGGATAGAGA; IFIT2-4 forward, TCCCAATCAAAATGGGAGTG, and IFIT2-4 reverse, TGTGGCAGGATCACTTATGAA; IFIT2-5 forward, CCAATCTGATAAAAGCTCAGAAA, and IFIT2-5 reverse, AGTTCTCCTTCATTTGCCTTT; IFIT2-6 forward, GCAGCCCTGGAATGCTTAC, and IFIT2-6 reverse, CAGGCATAGTTTCCCCAGGT; IFIT2 downstream forward, TGAGTCATAGTTTGTGTTATTTCTGA, and IFIT2 downstream reverse, GGATTCTGGAAAGGTAAAGAAAGA.

Transfection with siRNA

Transfection experiments were performed using the Lipofectamine RNAiMAX transfection reagents according to the manufacturer's instructions (Invitrogen). Cells were transfected with small interfering (si)RNA pools (all from Dharmacon) targeting the genes encoding human Top1, BRD4, CDK9, CCNT1, SMARCA2, SMARCA4, TOP2A, TOP2B, or with a control non-targeting pool, at the final concentration of 50 nM. Cells were used 48 hours after transfection, and the efficiency of gene knockdown was determined by qPCR or immunoblotting.

Microarray analysis

A549 cells were transfected with siRNA targeting the gene encoding Top1 or control non-targeting siRNA (siCtrl), then infected in triplicate with the PR8ΔNS1 virus (MOI = 3). Non-transfected cells were also infected, as a further control. RNA was isolated from infected and uninfected cells with a Qiagen RNeasy kit and 200 ng of RNA per sample was then used to prepare labeled RNA that was hybridized to Human HT-12 v4 Expression BeadChips (Illumina). Data were analyzed using the Genespring software (version 12.5).

To determine the effect of Top1 depletion on the magnitude of cell response during infection, raw signal values obtained from uninfected and infected cells in all siRNA treatments were quantile-normalized before being baseline-transformed to the medians of signal values for the corresponding uninfected siRNA-treated samples. For the identification of probe sets with statistically significant differences in magnitude of response ($P < 0.01$), the statistical ANOVA test followed by a post-hoc (Tukey's honest significant difference) test was conducted.

We selected genes differentially expressed after treatment with siTop1 using a threshold ≥1.5-fold change ($P < 0.01$) in their expression relative to siCtrl-treated cells. When indicated, infection-induced genes were identified as the ones showing a fold change ≥1.5 ($P < 0.01$) in their expression in infected-siCtrl-treated cells as compared to uninfected siCtrl-treated cells.

All computations of *P* values were subjected to multiple-testing correction using the Benjamini-Hochberg method. For purposes of presentation, genes represented by multiple probe sets in the microarray were plotted in the heat maps as the averaged values of those probe sets.

To determine the effect of Top1 depletion under basal conditions, raw signal values from uninfected siRNA-treated cells were quantile-normalized before being baseline-transformed to the median of all samples. A statistical ANOVA test followed by a post-hoc test was then conducted. Genes regulated by the siRNA targeting the Top1 gene were defined as genes with a fold change ≥1.5 ($P < 0.01$) in their expression as compared to the siCtrl-controls. Normalized signal-intensity values of a list of canonical housekeeping genes were also used to determine the overall effect of the depletion of Top1 in cells. A full list of the affected genes is shown in table S1.

The Ingenuity Pathways Analysis software (Ingenuity Systems) was used for the identification of canonical path-

ways that showed "enrichment" among groups of genes with significant changes in their expression by microarray analysis. The DAVID gene-ontology analysis helped to identify genes associated with cytokine activity (*53*, *54*). A right-tailed Fisher's exact test was used for calculation of *P* values determining the probability that each pathway assigned to a specific data set was due to chance alone.

Mice and related experiments

C57BL/6J female mice were purchased from The Jackson Laboratories and housed under specific pathogen-free conditions in the animal care facility at the Icahn School of Medicine at Mount Sinai (ISMMS). Mice were studied at 7–12 weeks of age. All experiments were approved by the institutional animal care and use committee and carried out in accordance with the 'Guide for the Care and Use of Laboratory Animals' (NIH publication 86-23, revised 1985).

For the septic shock model, mice were injected intraperitoneally (i.p.) with 10 mg/kg of ultra pure LPS (from *E.coli* 0111:B4 strain-TLR4 ligand, InvivoGen) resuspended in 200 μl of water. For the preventive protocol, one group of mice received, after isoflurane anesthesia, a first retro-orbital intravenous injection with a dose of 30 mg/kg of CPT 30 min before LPS treatment followed by an i.p. challenge with the same dose of CPT one hour after LPS injection.

For the acute liver failure model, mice were injected i.p. with a mixture of 5 mg of D-(+)-galactosamine (Sigma) and 500 ng of ultrapure LPS (Invivogen) (referred as D-GalN/LPS), in 200 μL of water. One group of mice was also injected i.p. with 110 mg/kg of CPT one hour before (preventive protocol) or 2 hours and 30 min after (therapeutic protocol) GalN/LPS treatment.

For the sepsis model using *Staphyloccocus aureus* infection (subsp. *aureus* Rosenbach, FDA 209P strain, ATCC) bacteria were grown in Bacto Tryptic Soy Broth (BDbioscience) until stationary phase, washed and suspended in PBS at $25x10^8$ bacteria/mL and mice intravenously injected with 200 μl of the bacterial suspension. We then started the treatment 3 hours after infection, when animals presented the first clinical signs of disease (ruffled fur, diminished activity, and hunched posture). One group of mice received a first dose of 30 mg/kg of CPT intravenously, followed by IP injections of 45 mg/kg of CPT 24 and 48 hours later.

For the co-infection model, the influenza virus PR8 (H1N1 PR8 A/Puerto Rico/8/1934 strain, kind gift from A. García-Sastre) was administered intranasally in sterile PBS in a volume of 50 μL at a titer of $0.3xLD_{50}$. Three days after Influenza infection, *S. aureus* stocks were grown until exponential phase and resuspended in sterile PBS in a volume of 50 μL containing $5x10^8$ bacteria/mouse for intranasal administration. Mice were anesthetized with ketamine-xylazine before all intranasal injections. One group of mouse received 75 mg/kg of CPT i.p. at 12, 24 and 36 hours after viral infections.

Survival significance in in vivo experiments was calculated using a Log-Rank Mantel-Cox Test with the Graphpad software Prism.

During all treatments, mice were daily weighted and monitored two to six times per day until the end of the experiment. We considered a loss >20% of the initial weight as humane end point, according to the policy of the institutional animal care and use committee at ISMMS. In case of survival, animals were under observation twice per day for the following month and every week for additional months. We did not detect any side effect of the CPT treatment in mice monitored for at least 3 months.

Quantitative PCR in tissue samples: Spleens and lungs were homogenized in 1 mL of TRIzol® Reagent (Life Technologies) using a mechanical homogenizer. RNA separation and isolation were performed using chloroform and isopropanol (both from Sigma), respectively, according to manufacturer's instructions (Life Technologies). cDNA synthesis and qPCR were performed as described above.

Cytokine detection: Quantitative mRNA analysis for inflammatory gene expression was conducted after RNA isolation from the spleens of untreated and CPT-treated mice 90 min after LPS injection.

To determine the cytokine concentration during the treatment, 50 μL of blood was collected retro-orbitally 4 hours after LPS injection. Serum and plasma were separated after centrifugation at 10,000 rpm for 10 min. Quantitative determination of GM-CSF, IL-1β, IL-6 and TNFα in mouse serum was performed using a Mouse Inflammatory Magnetic 4-Plex Panel (Novex Life Technology), according to the manufacturer's instructions. Data was acquired using a Luminex® 100/200™ plate reader.

Cell suspensions and ex-vivo re-stimulation: Cell suspensions were obtained after cutting the organs into small pieces followed by 30 min incubation at 37°C in DMEM containing 1 mg/mL collagenase D (Roche) and 20 μg/mL DNase (Roche). Tissue suspensions were then filtered through a 70 μm cell strainer (BD Falcon) and red blood cells were lysed using 1 mL of RBC Lysis Buffer (Affimetrix eBioscience).

For surface staining, cells were suspended in PBS containing 2% FBS, anti-mouse CD16/32 (Biolegend) and 0.1% NaN_3. For intracellular staining, cells were fixed in Fixation/Permeabilization buffer (eBioscience) and stained in Perm/Wash buffer (eBioscience).

For antigen specific re-stimulation, cells were resuspended in complete (*i.e.* supplemented with 10% FBS, 100 μg/mL penicillin, 100 μg/mL streptomycin, 1 nM sodium pyruvate) DMEM (Sigma) and restimulated with 100 nM of the peptide ASNENMETM derived from viral A/PR8/34 nu-

cleoprotein (NP, 366-374 aa) (MBL) in the presence of Brefeldin A (Biolegend), and incubated for 6 hours at 37°C.

All antibodies were purchased from Biolegend: anti-mouse CD45 (clone 30-F11), CD11c (N418), CD11b (M1/70), Ly6C (HK 4.1), CD69 (H1.2F3), MHC-II (M5/114.15.2), CD8β (Ly-3), CD44 (IM7), CD3ε (17A2), CD45 (30-F11), TNFα (MΠ6-XT22), IFNγ (XMG1.2). Dead cells were discriminated using the Zombie Aqua Fixable Viability Kit (Biolegend), referred to as Life/Death dye.

Acquisition of stained cells was made with a BD LSRII flow cytometer (BD Bioscience) and data was analyzed with FlowJo software (Treestar).

Antibodies and immunoblotting

Antibodies used were as follows: anti-β actin (3700; Cell Signaling); anti-TOP2A (ab52934; Abcam); anti-TOP2B (ab58442; Abcam); anti-TOP1 (A302-589A; Bethyl); anti-FLAG-HRP (A8592; Sigma). Gradient gels were used based on the molecular weight (MW) of the proteins to be evaluated followed by wet-transfer on PVDF membranes.

ChIP

The following antibodies were used: anti-RNA polymerase II (RNAPII) (clone 8WG16; Covance/BioLegend), anti-Topoisomerase I (TOP1) (rabbit polyclonal anti-human IgG; Bethyl Laboratories, Inc.; rabbit polyclonal anti-human/mouse serum; Abcam), anti-histone H3 (rabbit polyclonal IgG; Abcam), anti-TATA binding protein (rabbit polyclonal anti-serum; Abcam), and anti-Histone H4ac (rabbit polyclonal anti-human/mouse serum; Active Motif).

ChIP experiments were conducted as described (*55*). For experiments with ChIP followed by qPCR, a crosslinking was performed for 10 min. For sonication, we used a refrigerated Bioruptor (Diagenode), which we optimized to generate DNA fragments of approximately 200–1,000 base pair (bp). Lysates were pre-cleared for 3 hours using the appropriate isotype-matched control antibody (rabbit IgG; Cell Signaling) or anti-mouse IgG (Cell Signaling). The specific antibodies were coupled with magnetic paramagnetic beads (Dynabeads® M-280 Sheep anti-Mouse IgG; ThermoFisher Scientific) bound to anti–mouse IgG or anti–rabbit IgG for 6 hours. Antibody-bound beads and chromatin were then immune-precipitated overnight at 4°C with rotation. After washing, reverse crosslinking was carried out overnight at 65°C. After digestion with RNase and proteinase K (Roche), DNA was isolated with a MinElute kit (Qiagen) and used for downstream applications. The statistical significance of ChIP qPCR analysis was determined with a two-tailed Student's paired *t*-test.

ChIP-Seq sample preparation and sequencing

Following sonication using the Bioruptor Pico (Diagenode), input and IP samples were analyzed on an Agilent Bioanalyzer (DNA High Sensitivity kit) to confirm that the fragment distributions were within the expected size range. Sheared Input and ChIP DNA samples were then end-repaired using NEBNext® End Repair Module (New England BioLabs Inc.) and cleaned up using 1.5x AMPure XP beads (Beckman Coulter, Inc.) according to the manufacturer's instructions, except for the final elution step, which we omitted. Next, A-tailing was done on beads using the NEBNext® dA-Tailing Module (New England BioLabs Inc.), followed by addition of 20% polyethylene glycol (PEG)/NaCl in a 1.5x ratio to AMPure XP bead cleanup, again omitting the final elution step. Adaptor ligation was performed using the NEBNext® Quick Ligation Module (New England BioLabs Inc.) and 80 μM of DNA Multiplex Adaptor. Then, 20% PEG/NaCl was added in a 1.5x ratio followed by the AMPure XP cleanup. Samples were then eluted from beads and split into 2 aliquots. Each aliquot was amplified for 28 cycles using KAPA HiFi HotStart ReadyMix PCR Kit (Kapa Biosystems) and 25 μM of PE Forward primer, and 25 μM of an indexed Reverse primer. PCR reactions were cleaned using 1.5x of the AMPure XP beads according to the manufacturer's protocol and selected based on fragments with a size of 250-500nt on the BluePippin platform using 2% M1 Marker gels. Size selected libraries were cleaned using 1.8x of the AMPure XP beads and sequenced on the HiSEq. 2500 platform in a 100nt single-end read format.

Adapters used for ligation: Adapter1, 5′ P-GATCGGAAGAGCACACGTCT; Adapter2, 5′ ACACTCTTTCCCTACACGACGCTCTTCCGATC*T (* = phosphorothioate)

Barcode PCR primers:
5′AATGATACGGCGACCACCGAGATCTACACTCTTTCCCTA CACGACGCTCTTCCGATC*T,
5′CAAGCAGAAGACGGCATACGAGAT[NNNNNN]GTGACT GGAGTTCAGACGTGTGCTCTTCCGATC*T (where 'N' corresponds to the barcode sequences used).

ChIP-seq data processing

ChIP-Seq reads were trimmed for adapter sequences using 'cutadapt'. Reads were then filtered using 'sickle' with a minimum quality threshold of 20 and retaining only sequences containing at least 20 bases. QC-filtered reads were then aligned against the human reference genome (GRCh37) using STAR, selecting only non-ambiguous alignments and allowing up to 5 mismatches for each alignment. The resulting BAM files were processed using the R package "Pasha" with default parameters in order to exclude artefactual enrichments, estimate fragments elongation, and prepare genome-wide read coverage tracks in variable-step WIG

format. WIG scores were finally rescaled for each sample by dividing all values by the average genome wide enrichment value.

Average profile computation. The average read coverage for selected genes was calculated across the annotated gene regions including 2 kb flanking regions. For each gene, coverage in flanking regions was sampled across 167 equally spaced bins and the resulting values were averaged across the upstream and downstream regions of all selected genes. Coverage across the annotated region of each gene was calculated in 666 equally spaced bins within the annotated start and end coordinates and the resulting vectors were averaged across all genes and combined with the gene-flanking regions to create a composite average profile of 1000 points covering selected annotations and 2kb of each flanking region. All average profiles were normalized based on the average ChIP signal across the third quartile (i.e., last 50-75%) of the gene body of active genes (previously identified by Gro-Seq profiling (*56*)), to account for differences in ChIP-efficiency between experiments.

Chemical synthesis of topotecan-alkyne

An alkyne group was introduced to the 10-hydroxyl group of TPT through a Mitsunobu reaction (*57*), as the 10-hydroxyl of topotecan does not contribute to the binding between human topoisomerase I covalently joined to double-stranded DNA and topotecan (according to the reported x-ray crystal structure (*58*)). Topotecan hydrochloride was dissolved in distilled water and further neutralized by adding (dropwise) a saturated solution of sodium bicarbonate ($NaHCO_3$) until the pH reached 9-10. Hydrochloride-free topotecan was extracted from this solution by washing the aqueous phase with dichloromethane (DCM) 3 times, combining the organic phase, drying it by incubation with sodium sulfate (Na_2SO_4) for one hour, and finally evaporating DCM under reduced pressure. The topotecan was then fully dissolved together with 5 eq. triphenylphospine (Ph_3P) and 5 eq. propargyl alcohol in a small volume of anhydrous tetrahydrofuran (THF). Five eq. of diethyl azodicarboxylate (DEAD) was then added dropwise into the solution. The reaction was monitored using thin layer chromotography (TLC). The reaction time was 2 hours at room temperature. The solvents were removed by using a rotary evaporator (Rotovap). The product was purified by applying preparative HPLC with a gradient elution consisting of methanol (MeOH) and H_2O. Purity was ≥ 95% and the rude yield was 74%. ^{1}HNMR (MeOH-d_6, 600 MHz): δ 8.95 (1H, s), 8.43 (1H, d, J = 9.5 Hz), 8.02 (1H, d, J = 9.5 Hz), 7.68 (1H, s), 5.61 (1H, d, J = 16.2 Hz), 5.43 (1H, d, J = 16.2 Hz), 5.39 (2H, s), 5.20 (2H, d, J = 2.1 Hz), 4.18 (2H, s), 3.31 (1H, s), 3.03 (6H, s), 1.99 (2H, m), 1.04 (3H, t, J = 7.3 Hz). Calculation for $C_{26}H_{26}N_3O_5$, $[M+H]^+$, and $C_{52}H_{51}N_6O_{10}$, $[2M+H]^+$, were 460.1871 and 919.3667, respectively, 460.2103 and 919.3643 were found in HRMS (*59*). All chemical reagents and solvents were commercially purchased from Sigma-Aldrich.

Chemical immunoprecipitation (chem-ChIP)

A549 cells (10^8 cells/condition) were pre-treated for one hour with 100 nM of Topotecan-Alkyne (TPT-A) or DMSO, infected with influenza PR8ΔNS1 virus and at one hour post-infection, treated again with TPT-A or DMSO. Cells were collected at 6 hours p.i. and treated as described above for the ChIP procedure. Sonicated DNA fragments for each condition were separated into 500 μL aliquots. The following reagents were added sequentially with vortexing after each addition: 11.3 μL of 5 mM biotin-azide (final concentration: 100 μM), 11.3 μL of 50 mM tris (2-carboxyethyl) phosphine (TCEP, final concentration: 1 mM), 34 μL of 1.7 mM tris (benzyltriazolylmethyl) amine (TBTA, final concentration: 100 μM), and 11.3 μL of 50 mM copper(II) sulfate pentahydrate ($CuSO4{\cdot}5H_2O$, final concentration: 1 mM). These mixtures were then incubated at room temperature for one hour, with vortexing after the first 30 min. Chromatin aliquots were combined and centrifuged for 5 min at 6,500 g at 4°C. The supernatant was then removed for downstream immunoprecipitation. ChIP qPCR was performed as described above. The statistical significance of ChIP qPCR analysis was determined with a two-tailed Student's paired *t*-test.

Stranded RNA-sequencing and data analysis

1 μg of RNA was treated using the Ribo-Zero Gold rRNA Removal Kit (Human/Mouse/Rat, Illumina), and purified post-depletion with 1.6x ratio of AMPureXP beads. Directional RNA libraries were prepared using NEBNext Ultra Directional RNA library prep kit for Illumina (New England BioLabs Inc.), according to manufacturer's instruction. Fragment size distribution and concentration of the PCR amplified libraries were assessed using the Qubit and the Agilent Bioanalyzer. Finally, samples were sequenced on the HiSEq. 2500 platform in a 100bp single-end read format.

Following adapter removal with cutadapt and base quality trimming to remove 3′ ends if more than 20 bases with Q<20 were present, reads were mapped to the human (hg19) and Ebola virus (H.sapiens-tc/COD/1976/Yambuku-Mayinga, NC_002549) reference genomes using STAR (*60*) and gene- and transcript count summaries were generated using Featurecounts (*61*). Read counts were then combined into a numeric matrix with genes in rows and experiments in columns, and used as input for differential gene expression analysis with the Bioconductor edgeR package (*62*). Normalization factors were computed using the weighted Trimmed Mean of M-values (TMM), and dispersions (common, trended, and tagwise) were estimated before fitting a negative

binomial General Linerized Model that accounted for experimental conditions with 2 biological replicates each. Finally, a likelihood ratio test was carried against selected contrasts. P-values were corrected for multiple testing using the Benjamin-Hochberg (BH) method and used to select genes with significant expression differences (FDR q < 0.05).

Proteomic analysis

A549 cells were treated with CPT or DMSO and infected with the influenza PR8ΔNS1 virus as described above, collected at 6 hours p.i., washed 3 times with PBS (including protease inhibitors (Roche)), then frozen as cell pellets. These pellets were sent to Bioproximity LLC, where global proteomic profiling was acquired using an ultra-performance liquid chromatography tandem mass-spectrometry (UPLC-MS/MS).

For the analysis of mass spectrometry "hits," initial thresholds were calculated in duplicate experiments for protein abundances in both DMSO and CPT treated, uninfected cells. Next, protein abundances were calculated in the respective infected conditions, and normalized using non-infected abundances. We considered upregulated hits as having a normalized unique protein score above 5 in the DMSO treated, infected cells. The statistical comparison between normalized infected identifications was determined with a two-tailed Student's *t* test under the assumption of equal variances between groups.

Transcription factor promoter enrichment analysis

Identification of transcription factors (TFs) regulating the genes affected by Top1 depletion was performed using a computational method that overlaps the genomic coordinates of a set of gene promoters with a large library of TF-genome interactions. We created the ChIP-seq library by compiling 1,630 human ChIP-seq datasets from a variety of sources, including ENCODE (*63*), Cistrome (*64*), PAZAR (*65*), and Re-Map (*66*). As input, we took a set of genomic regions of interest (e.g., promoters of genes whose expression changes upon silencing of Top1) that we systematically overlapped with each ChIP-seq dataset and we counted the number of input regions overlapped by at least one base.

Next, a P-value describing the significance of this overlap was estimated using a simulation-based procedure: a distribution of *expected overlap* values was created from 1,000 iterations of randomly choosing RefSeq gene promoters with the same length as the input set (as an example, for 50 promoters of length 100 bp as input, 50 randomly chosen promoters of length 100 bp were used in each simulation). The distribution of the expected overlap values from the randomized data resembled a normal distribution, and was used to generate a Z-score and P-value estimating the significance of the observed number of input regions that overlapped each ChIP-seq dataset. We obtained a ranked list of TFs, based on experimentally-determined binding sites located in the promoters of each gene set. We applied this procedure to each input gene list using 3 different promoter definitions: (-100,+1), (-1000,+1), and (-10000,+1), relative to the transcription start site. Results were similar regardless of promoter length (table S3). We further annotated the results with TF binding site motif enrichment scores (using the same promoter definitions). For this, we used the HOMER motif enrichment algorithm (*67*), and a large library of human position weight matrices obtained from the CisBP database (*68*).

Mapping

ChIP-Seq data from this study and publicly available data from ENCODE for DNase-Seq (GSE26328) and H3K27ac (GSE29611) in A549 cells were aligned to the human genome (hg19/GRCh37) using Bowtie2 with default parameters (*69*). Only reads that mapped to unique genomic positions were considered for downstream analysis. Normalized promoter ChIP-seq read densities were calculated using HOMER (http://homer.salk.edu/) by counting the total number of reads per 10^7 aligned reads from each experiment found from -500 to +500 bp relative to the representative RefSeq defined transcription start site (TSS) for each gene (*67*). META gene plots were compiled by calculating ChIP-seq read densities along RefSeq gene bodies (>3kb in length) using HOMER. CpG Island promoters were defined by RefSeq TSS found within 200 bp of an annotated CpG Island (*70*). IFN-stimulated response elements (IRSE) containing promoters were defined by searching for ISRE motifs from -500 to +100 relative to the TSS using HOMER.

REFERENCES AND NOTES

1. C. A. Janeway Jr., R. Medzhitov, Innate immune recognition. *Annu. Rev. Immunol.* **20**, 197–216 (2002). Medline doi:10.1146/annurev.immunol.20.083001.084359
2. R. Medzhitov, Approaching the asymptote: 20 years later. *Immunity* **30**, 766–775 (2009). Medline doi:10.1016/j.immuni.2009.06.004
3. B. Beutler, C. Eidenschenk, K. Crozat, J. L. Imler, O. Takeuchi, J. A. Hoffmann, S. Akira, Genetic analysis of resistance to viral infection. *Nat. Rev. Immunol.* **7**, 753–766 (2007). Medline doi:10.1038/nri2174
4. J. W. Schoggins, S. J. Wilson, M. Panis, M. Y. Murphy, C. T. Jones, P. Bieniasz, C. M. Rice, A diverse range of gene products are effectors of the type I interferon antiviral response. *Nature* **472**, 481–485 (2011). Medline doi:10.1038/nature09907
5. Y. J. Crow, Type I interferonopathies: Mendelian type I interferon up-regulation. *Curr. Opin. Immunol.* **32**, 7–12 (2015). Medline doi:10.1016/j.coi.2014.10.005
6. T. Hanada, A. Yoshimura, Regulation of cytokine signaling and inflammation. *Cytokine Growth Factor Rev.* **13**, 413–421 (2002). Medline doi:10.1016/S1359-6101(02)00026-6
7. F. McNab, K. Mayer-Barber, A. Sher, A. Wack, A. O'Garra, Type I interferons in infectious disease. *Nat. Rev. Immunol.* **15**, 87–103 (2015). Medline doi:10.1038/nri3787
8. M. Brandes, F. Klauschen, S. Kuchen, R. N. Germain, A systems analysis identifies a feedforward inflammatory circuit leading to lethal influenza infection. *Cell* **154**, 197–212 (2013). Medline doi:10.1016/j.cell.2013.06.013
9. Y. M. Loo, M. Gale Jr., Influenza: Fatal immunity and the 1918 virus. *Nature* **445**, 267–268 (2007). Medline doi:10.1038/445267a

10. P. A. Ward, New approaches to the study of sepsis. *EMBO Mol. Med.* **4**, 1234–1243 (2012). Medline doi:10.1002/emmm.201201375
11. L. Strähle, D. Garcin, P. Le Mercier, J. F. Schlaak, D. Kolakofsky, Sendai virus targets inflammatory responses, as well as the interferon-induced antiviral state, in a multifaceted manner. *J. Virol.* **77**, 7903–7913 (2003). Medline doi:10.1128/JVI.77.14.7903-7913.2003
12. G. L. Beretta, L. Gatti, P. Perego, N. Zaffaroni, Camptothecin resistance in cancer: Insights into the molecular mechanisms of a DNA-damaging drug. *Curr. Med. Chem.* **20**, 1541–1565 (2013). Medline doi:10.2174/0929867311320120006
13. Y. Chen, S. H. Yang, D. Y. Hueng, J. P. Syu, C. C. Liao, Y. C. Wu, Cordycepin induces apoptosis of C6 glioma cells through the adenosine 2A receptor-p53-caspase-7-PARP pathway. *Chem. Biol. Interact.* **216**, 17–25 (2014). Medline doi:10.1016/j.cbi.2014.03.010
14. S. Kubicek, R. J. O'Sullivan, E. M. August, E. R. Hickey, Q. Zhang, M. L. Teodoro, S. Rea, K. Mechtler, J. A. Kowalski, C. A. Homon, T. A. Kelly, T. Jenuwein, Reversal of H3K9me2 by a small-molecule inhibitor for the G9a histone methyltransferase. *Mol. Cell* **25**, 473–481 (2007). Medline doi:10.1016/j.molcel.2007.01.017
15. I. Kubo, T. J. Ha, K. Shimizu, Lipoxygenase inhibitory activity of 6-pentadecanylsalicylic acid without prooxidant effect. *Nat. Prod. Commun.* **5**, 85–90 (2010). Medline
16. S. Menazza, B. Blaauw, T. Tiepolo, L. Toniolo, P. Braghetta, B. Spolaore, C. Reggiani, F. Di Lisa, P. Bonaldo, M. Canton, Oxidative stress by monoamine oxidases is causally involved in myofiber damage in muscular dystrophy. *Hum. Mol. Genet.* **19**, 4207–4215 (2010). Medline doi:10.1093/hmg/ddq339
17. P. B. Rahl, C. Y. Lin, A. C. Seila, R. A. Flynn, S. McCuine, C. B. Burge, P. A. Sharp, R. A. Young, c-Myc regulates transcriptional pause release. *Cell* **141**, 432–445 (2010). Medline doi:10.1016/j.cell.2010.03.030
18. K. M. Regal, S. L. Mercer, J. E. Deweese, HU-331 is a catalytic inhibitor of topoisomerase IIα. *Chem. Res. Toxicol.* **27**, 2044–2051 (2014). Medline doi:10.1021/tx500245m
19. N. A. Smith, J. A. Byl, S. L. Mercer, J. E. Deweese, N. Osheroff, Etoposide quinone is a covalent poison of human topoisomerase IIβ. *Biochemistry* **53**, 3229–3236 (2014). Medline doi:10.1021/bi500421q
20. Q. Zhou, T. Li, D. H. Price, RNA polymerase II elongation control. *Annu. Rev. Biochem.* **81**, 119–143 (2012). Medline doi:10.1146/annurev-biochem-052610-095910
21. P. Filippakopoulos, S. Knapp, Targeting bromodomains: Epigenetic readers of lysine acetylation. *Nat. Rev. Drug Discov.* **13**, 337–356 (2014). Medline doi:10.1038/nrd4286
22. Y. Pommier, Topoisomerase I inhibitors: Camptothecins and beyond. *Nat. Rev. Cancer* **6**, 789–802 (2006). Medline doi:10.1038/nrc1977
23. E. Nicodeme, K. L. Jeffrey, U. Schaefer, S. Beinke, S. Dewell, C. W. Chung, R. Chandwani, I. Marazzi, P. Wilson, H. Coste, J. White, J. Kirilovsky, C. M. Rice, J. M. Lora, R. K. Prinjha, K. Lee, A. Tarakhovsky, Suppression of inflammation by a synthetic histone mimic. *Nature* **468**, 1119–1123 (2010). Medline doi:10.1038/nature09589
24. P. Filippakopoulos, J. Qi, S. Picaud, Y. Shen, W. B. Smith, O. Fedorov, E. M. Morse, T. Keates, T. T. Hickman, I. Felletar, M. Philpott, S. Munro, M. R. McKeown, Y. Wang, A. L. Christie, N. West, M. J. Cameron, B. Schwartz, T. D. Heightman, N. La Thangue, C. A. French, O. Wiest, A. L. Kung, S. Knapp, J. E. Bradner, Selective inhibition of BET bromodomains. *Nature* **468**, 1067–1073 (2010). Medline doi:10.1038/nature09504
25. G. Egger, G. Liang, A. Aparicio, P. A. Jones, Epigenetics in human disease and prospects for epigenetic therapy. *Nature* **429**, 457–463 (2004). Medline doi:10.1038/nature02625
26. K. T. Atherton, D. C. Burke, Interferon induction by viruses and polynucleotides: A differential effect of comptothecin. *J. Gen. Virol.* **29**, 297–304 (1975). Medline doi:10.1099/0022-1317-29-3-297
27. K. T. Atherton, D. C. Burke, The effects of some differential metabolic inhibitors on interferon superinduction. *J. Gen. Virol.* **41**, 2 (1975).
28. W. F. Chiou, C. J. Chou, C. F. Chen, Camptothecin suppresses nitric oxide biosynthesis in RAW 264.7 macrophages. *Life Sci.* **69**, 625–635 (2001). Medline doi:10.1016/S0024-3205(01)01154-7
29. I. F. King, C. N. Yandava, A. M. Mabb, J. S. Hsiao, H. S. Huang, B. L. Pearson, J. M. Calabrese, J. Starmer, J. S. Parker, T. Magnuson, S. J. Chamberlain, B. D. Philpot, M. J. Zylka, Topoisomerases facilitate transcription of long genes linked to autism. *Nature* **501**, 58–62 (2013). Medline doi:10.1038/nature12504
30. S. Solier, M. C. Ryan, S. E. Martin, S. Varma, K. W. Kohn, H. Liu, B. R. Zeeberg, Y. Pommier, Transcription poisoning by Topoisomerase I is controlled by gene length, splice sites, and miR-142-3p. *Cancer Res.* **73**, 4830–4839 (2013). Medline doi:10.1158/0008-5472.CAN-12-3504
31. F. Kouzine, A. Gupta, L. Baranello, D. Wojtowicz, K. Ben-Aissa, J. Liu, T. M. Przytycka, D. Levens, Transcription-dependent dynamic supercoiling is a short-range genomic force. *Nat. Struct. Mol. Biol.* **20**, 396–403 (2013). Medline doi:10.1038/nsmb.2517
32. M. Kretzschmar, M. Meisterernst, R. G. Roeder, Identification of human DNA topoisomerase I as a cofactor for activator-dependent transcription by RNA polymerase II. *Proc. Natl. Acad. Sci. U.S.A.* **90**, 11508–11512 (1993). Medline doi:10.1073/pnas.90.24.11508
33. A. Merino, K. R. Madden, W. S. Lane, J. J. Champoux, D. Reinberg, DNA topoisomerase I is involved in both repression and activation of transcription. *Nature* **365**, 227–232 (1993). Medline doi:10.1038/365227a0
34. K. W. Kohn, Y. Pommier, Molecular and biological determinants of the cytotoxic actions of camptothecins. Perspective for the development of new topoisomerase I inhibitors. *Ann. N.Y. Acad. Sci.* **922**, 11–26 (2000). Medline doi:10.1111/j.1749-6632.2000.tb07021.x
35. S. Höing, Y. Rudhard, P. Reinhardt, M. Glatza, M. Stehling, G. Wu, C. Peiker, A. Böcker, J. A. Parga, E. Bunk, J. C. Schwamborn, M. Slack, J. Sterneckert, H. R. Schöler, Discovery of inhibitors of microglial neurotoxicity acthing thorugh multiple mechanisms using a stem-cell-based phenotypic assay. *Cell Stem Cell* **11**, 620–632 (2012). Medline doi:10.1016/j.stem.2012.07.005
36. R. Madabhushi, F. Gao, A. R. Pfenning, L. Pan, S. Yamakawa, J. Seo, R. Rueda, T. X. Phan, H. Yamakawa, P. C. Pao, R. T. Stott, E. Gjoneska, A. Nott, S. Cho, M. Kellis, L. H. Tsai, Activity-induced DNA breaks govern the expression of neuronal early-reponse genes. *Cell* **161**, 1592–1605 (2015). Medline doi:10.1016/j.cell.2015.05.032
37. L. Anders, M. G. Guenther, J. Qi, Z. P. Fan, J. J. Marineau, P. B. Rahl, J. Lovén, A. A. Sigova, W. B. Smith, T. I. Lee, J. E. Bradner, R. A. Young, Genome-wide localization of small molecules. *Nat. Biotechnol.* **32**, 92–96 (2014). Medline doi:10.1038/nbt.2776
38. S. S. Teves, S. Henikoff, Transcription-generated torsional stress destabilizes nucleosomes. *Nat. Struct. Mol. Biol.* **21**, 88–94 (2014). Medline doi:10.1038/nsmb.2723
39. V. R. Ramirez-Carrozzi, A. A. Nazarian, C. C. Li, S. L. Gore, R. Sridharan, A. N. Imbalzano, S. T. Smale, Selective and antagonistic functions of SWI/SNF and Mi-2β nucleosome remodeling complexes during an inflammatory response. *Genes Dev.* **20**, 282–296 (2006). Medline doi:10.1101/gad.1383206
40. V. R. Ramirez-Carrozzi, D. Braas, D. M. Bhatt, C. S. Cheng, C. Hong, K. R. Doty, J. C. Black, A. Hoffmann, M. Carey, S. T. Smale, A unifying model for the selective regulation of inducible transcription by CpG islands and nucleosome remodeling. *Cell* **138**, 114–128 (2009). Medline doi:10.1016/j.cell.2009.04.020
41. D. C. Hargreaves, T. Horng, R. Medzhitov, Control of inducible gene expression by signal-dependent transcriptional elongation. *Cell* **138**, 129–145 (2009). Medline doi:10.1016/j.cell.2009.05.047
42. S. T. Smale, G. Natoli, Transcriptional control of inflammatory responses. *Cold Spring Harb. Perspect. Biol.* **6**, a016261 (2014). Medline doi:10.1101/cshperspect.a016261
43. S. Akira, S. Uematsu, O. Takeuchi, Pathogen recognition and innate immunity. *Cell* **124**, 783–801 (2006). Medline doi:10.1016/j.cell.2006.02.015
44. H. K. Kim, D. Missiakas, O. Schneewind, Mouse models for infectious diseases caused by *Staphylococcus aureus*. *J. Immunol. Methods* **410**, 88–99 (2014). doi:10.1016/j.jim.2014.04.007
45. J. A. McCullers, J. L. McAuley, S. Browall, A. R. Iverson, K. L. Boyd, B. Henriques Normark, Influenza enhances susceptibility to natural acquisition of and disease due to *Streptococcus pneumoniae* in ferrets. *J. Infect. Dis.* **202**, 1287–1295 (2010). Medline doi:10.1086/656333
46. G. Sass, K. Koerber, R. Bang, H. Guehring, G. Tiegs, Inducible nitric oxide synthase is critical for immune-mediated liver injury in mice. *J. Clin. Invest.* **107**, 439–447 (2001). Medline doi:10.1172/JCI10613
47. M. Bray, S. Mahanty, Ebola hemorrhagic fever and septic shock. *J. Infect. Dis.*

188, 1613–1617 (2003). Medline doi:10.1086/379727
48. L. Martínez-Gil, J. Ayllon, M. B. Ortigoza, A. García-Sastre, M. L. Shaw, P. Palese, Identification of small molecules with type I interferon inducing properties by high-throughput screening. *PLOS ONE* **7**, e49049 (2012). Medline doi:10.1371/journal.pone.0049049
49. A. Baum, R. Sachidanandam, A. García-Sastre, Preference of RIG-I for short viral RNA molecules in infected cells revealed by next-generation sequencing. *Proc. Natl. Acad. Sci. U.S.A.* **107**, 16303–16308 (2010). Medline doi:10.1073/pnas.1005077107
50. L. Martínez-Sobrido, R. Cadagan, J. Steel, C. F. Basler, P. Palese, T. M. Moran, A. García-Sastre, Hemagglutinin-pseudotyped green fluorescent protein-expressing influenza viruses for the detection of influenza virus neutralizing antibodies. *J. Virol.* **84**, 2157–2163 (2010). Medline doi:10.1128/JVI.01433-09
51. L. Martínez-Gil, P. H. Goff, R. Hai, A. García-Sastre, M. L. Shaw, P. Palese, A Sendai virus-derived RNA agonist of RIG-I as a virus vaccine adjuvant. *J. Virol.* **87**, 1290–1300 (2013). Medline doi:10.1128/JVI.02338-12
52. C. F. Basler, X. Wang, E. Mühlberger, V. Volchkov, J. Paragas, H. D. Klenk, A. García-Sastre, P. Palese, The Ebola virus VP35 protein functions as a type I IFN antagonist. *Proc. Natl. Acad. Sci. U.S.A.* **97**, 12289–12294 (2000). Medline doi:10.1073/pnas.220398297
53. W. Huang, B. T. Sherman, R. A. Lempicki, Systematic and integrative analysis of large gene lists using DAVID bioinformatics resources. *Nat. Protoc.* **4**, 44–57 (2009). Medline doi:10.1038/nprot.2008.211
54. W. Huang, B. T. Sherman, R. A. Lempicki, Bioinformatics enrichment tools: Paths toward the comprehensive functional analysis of large gene lists. *Nucleic Acids Res.* **37**, 1–13 (2009). Medline doi:10.1093/nar/gkn923
55. T. I. Lee, S. E. Johnstone, R. A. Young, Chromatin immunoprecipitation and microarray-based analysis of protein location. *Nat. Protoc.* **1**, 729–748 (2006). Medline doi:10.1038/nprot.2006.98
56. M. S. Miller, A. Rialdi, J. S. Ho, M. Tilove, L. Martinez-Gil, N. P. Moshkina, Z. Peralta, J. Noel, C. Melegari, A. M. Maestre, P. Mitsopoulos, J. Madrenas, S. Heinz, C. Benner, J. A. Young, A. R. Feagins, C. F. Basler, A. Fernandez-Sesma, O. J. Becherel, M. F. Lavin, H. van Bakel, I. Marazzi, Senataxin suppresses the antiviral transcriptional response and controls viral biogenesis. *Nat. Immunol.* **16**, 485–494 (2015). Medline doi:10.1038/ni.3132
57. K. C. Swamy, N. N. Kumar, E. Balaraman, K. V. Kumar, Mitsunobu and related reactions: Advances and applications. *Chem. Rev.* **109**, 2551–2651 (2009). Medline doi:10.1021/cr800278z
58. B. L. Staker, K. Hjerrild, M. D. Feese, C. A. Behnke, A. B. Burgin Jr., L. Stewart, The mechanism of topoisomerase I poisoning by a camptothecin analog. *Proc. Natl. Acad. Sci. U.S.A.* **99**, 15387–15392 (2002). Medline doi:10.1073/pnas.242259599
59. K. Hyz, R. Kawecki, E. Bednarek, W. Bocian, J. Sitkowski, L. Kozerski, Topotecan dynamics, tautomerism and reactivity—1H/13C NMR and ESI MS study. *Magn. Reson. Chem.* **48**, 575–584 (2010). Medline
60. A. Dobin, C. A. Davis, F. Schlesinger, J. Drenkow, C. Zaleski, S. Jha, P. Batut, M. Chaisson, T. R. Gingeras, STAR: Ultrafast universal RNA-seq aligner. *Bioinformatics* **29**, 15–21 (2013). Medline doi:10.1093/bioinformatics/bts635
61. Y. Liao, G. K. Smyth, W. Shi, featureCounts: An efficient general purpose program for assigning sequence reads to genomic features. *Bioinformatics* **30**, 923–930 (2014). Medline doi:10.1093/bioinformatics/btt656
62. M. D. Robinson, D. J. McCarthy, G. K. Smyth, edgeR: A Bioconductor package for differential expression analysis of digital gene expression data. *Bioinformatics* **26**, 139–140 (2010). Medline doi:10.1093/bioinformatics/btp616
63. ENCODE Project Consortium, An integrated encyclopedia of DNA elements in the human genome. *Nature* **489**, 57–74 (2012). Medline
64. T. Liu, J. A. Ortiz, L. Taing, C. A. Meyer, B. Lee, Y. Zhang, H. Shin, S. S. Wong, J. Ma, Y. Lei, U. J. Pape, M. Poidinger, Y. Chen, K. Yeung, M. Brown, Y. Turpaz, X. S. Liu, Cistrome: An integrative platform for transcriptional regulation studies. *Genome Biol.* **12**, R83 (2011). Medline doi:10.1186/gb-2011-12-8-r83
65. E. Portales-Casamar, D. Arenillas, J. Lim, M. I. Swanson, S. Jiang, A. McCallum, S. Kirov, W. W. Wasserman, The PAZAR database of gene regulatory information coupled to the ORCA toolkit for the study of regulatory sequences. *Nucleic Acids Res.* **37**, D54–D60 (2009). Medline doi:10.1093/nar/gkn783
66. A. Griffon, Q. Barbier, J. Dalino, J. van Helden, S. Spicuglia, B. Ballester, Integrative analysis of public ChIP-seq experiments reveals a complex multi-cell regulatory landscape. *Nucleic Acids Res.* **43**, e27 (2015). Medline doi:10.1093/nar/gku1280
67. S. Heinz, C. Benner, N. Spann, E. Bertolino, Y. C. Lin, P. Laslo, J. X. Cheng, C. Murre, H. Singh, C. K. Glass, Simple combinations of lineage-determining transcription factors prime cis-regulatory elements required for macrophage and B cell identities. *Mol. Cell* **38**, 576–589 (2010). Medline doi:10.1016/j.molcel.2010.05.004
68. M. T. Weirauch, A. Yang, M. Albu, A. G. Cote, A. Montenegro-Montero, P. Drewe, H. S. Najafabadi, S. A. Lambert, I. Mann, K. Cook, H. Zheng, A. Goity, H. van Bakel, J. C. Lozano, M. Galli, M. G. Lewsey, E. Huang, T. Mukherjee, X. Chen, J. S. Reece-Hoyes, S. Govindarajan, G. Shaulsky, A. J. Walhout, F. Y. Bouget, G. Ratsch, L. F. Larrondo, J. R. Ecker, T. R. Hughes, Determination and inference of eukaryotic transcription factor sequence specificity. *Cell* **158**, 1431–1443 (2014). Medline doi:10.1016/j.cell.2014.08.009
69. B. Langmead, S. L. Salzberg, Fast gapped-read alignment with Bowtie 2. *Nat. Methods* **9**, 357–359 (2012). Medline doi:10.1038/nmeth.1923
70. M. Gardiner-Garden, M. Frommer, CpG islands in vertebrate genomes. *J. Mol. Biol.* **196**, 261–282 (1987). Medline doi:10.1016/0022-2836(87)90689-9

ACKNOWLEDGMENTS

We thank P. Palese for the FF-luciferase construct, chromatized cells, and Sendai virus, F. Kramer for the H3N2 virus, Richard Cadagan for help with virus propagations, T. Kraus for the use of the Luminex® 100/200™ plate reader, M. Schotsaert for help with co-infection experiments, S. Tripathi for providing IRF3-dependency data, the Genomics facility at Icahn School of Medicine at Mount Sinai, Bioproximity, LLC for proteomics work, J.K. Gregory for help with computer graphics, and H. Nakano for discussion about the history of Top1 inhibitors. Ivan Marazzi and Minji Byun designed the graphical abstract illustration of the 'The Vitruvian automaton'. The illustration is our homage to Marcus Vitruvius Pollio, Leonardo da Vinci, and the history of automata. The data presented in this manuscript are tabulated in the main paper and in the supplementary materials. Sequencing data are available in GEO, GSE52937 and linked superseries. Supported by the computational resources and staff of the Department of Scientific Computing at the Icahn School of Medicine at Mount Sinai; A.G.S, G.M., H.vB. and I.M. are partially supported by HHSN272201400008C - Center for Research on Influenza Pathogenesis (CRIP) a NIAID-funded Center of Excellence for Influenza Research and Surveillance (CEIRS). A.R. is supported in part by a Public Health Service Institutional Research Training Award (AI07647). A patent application (62/267,608) was filed by Mount Sinai related to treatment of inflammatory diseases with Top1 inhibitors. I.M. is supported in part by The Department of Defense W911NF-14-1-0353 (to I.M.) and by NIH grants U19AI106754 (to I.M. and A.G-S.), 1R01AN3663134 (to I.M and H.vB) and 1R56AI114770-01A1 (to I. M.)

SUPPLEMENTARY MATERIALS

www.sciencemag.org/cgi/content/full/science.aad7993/DC1
Figs. S1 to S15
Tables S1 to S4

3 November 2015; accepted 6 April 2016
Published online 28 April 2016
10.1126/science.aad7993

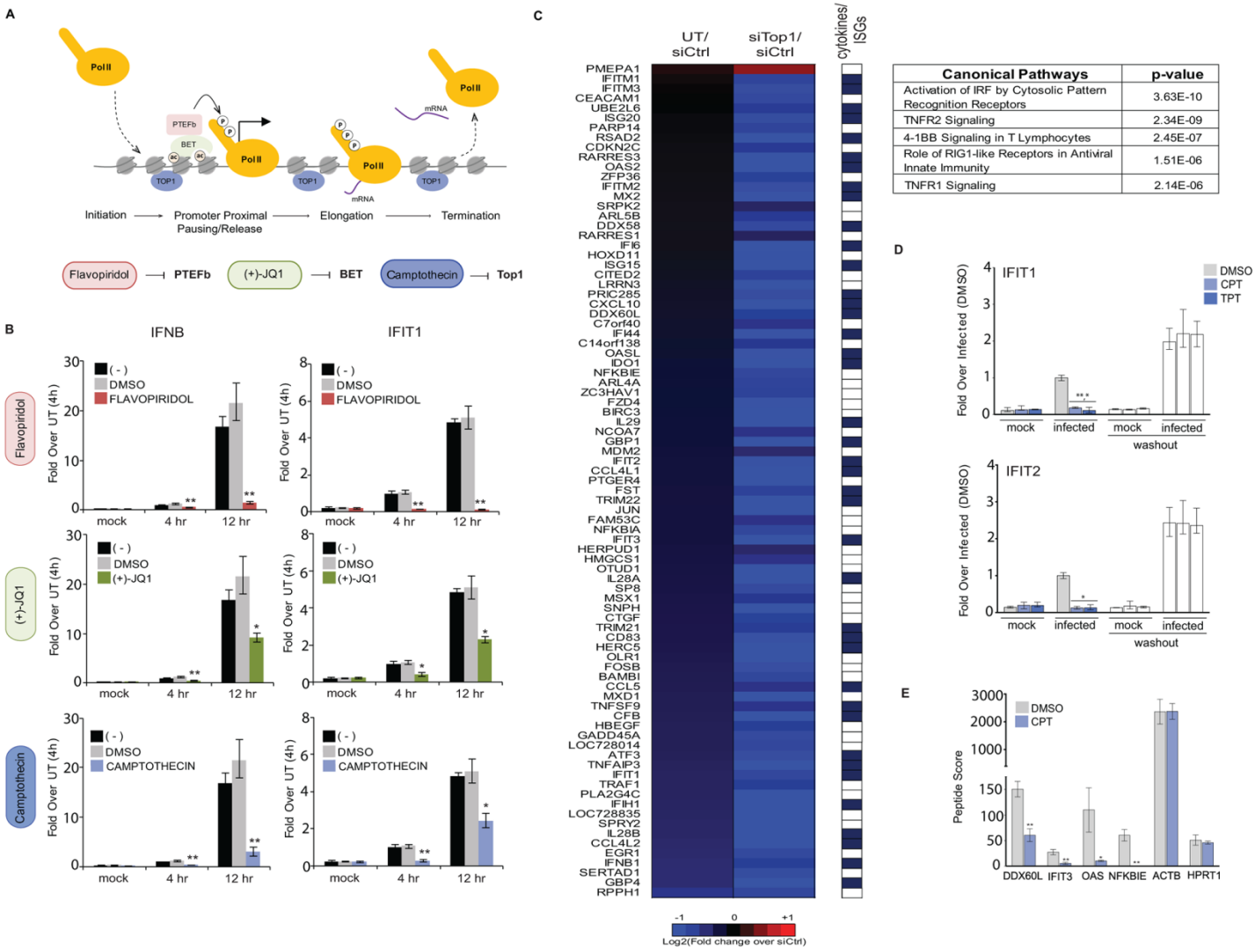

Fig. 1. Top1 inhibition suppresses PAMP-induced gene expression. (**A**) Schematic representation of factors controlling different phases of RNA polymerase II (RNAPII) mediated transcription. Chemical inhibitors Flavopiridol (red), (+)-JQ1 (green) and Camptothecin (blue, CPT) are color-coded according to their protein targets. (**B**) Quantitative PCR (qPCR) results showing the expression levels of representative viral PAMP-induced genes IFNB and IFIT1, in response to the influenza PR8ΔNS1 virus infection in untreated (-), DMSO, or 5 μM inhibitors treated A549 cells. (**C**) Heatmap showing fold change in gene expression levels in A549 cells not transfected (UT) or transfected with a Top1-specific siRNA (siTop1) as compared to non-targeting control siRNA treated (siCtrl) cells during infection with influenza PR8ΔNS1 for genes differentially expressed between siTop1 and siCtrl at 4 hours post-infection (p.i.) ($p < 0.01$; ANOVA with post-hoc TUKEY HSD test). Known interferon-stimulated (ISGs) and cytokine coding genes are indicated in the adjacent heatmap. A table summarizing the top five pathways affected by Top1 depletion during infection is also shown (top right). (**D**) Expression levels of IFIT1 and IFIT2 genes in response to influenza PR8ΔNS1 infection in A549 cells treated with 0.5 μM of CPT, 100 nM Topotecan (TPT) or DMSO at 4 hours p.i. (left bars) or 16 hours after washout (white, right bars). (**E**) Mass-spectrometry data showing representative virus-induced and housekeeping protein levels in response to influenza PR8ΔNS1 infection in A549 cells treated with 0.5 μM of CPT or DMSO at 6 hours p.i . *$P < 0.05$ and **$P < 0.005$ (calculated with a student's *t* test; with Holm-Bonferroni sequential correction). Data are from three [(B) to (D)] and two (E) independent experiments. Mean and standard deviation (s.d) are indicated.

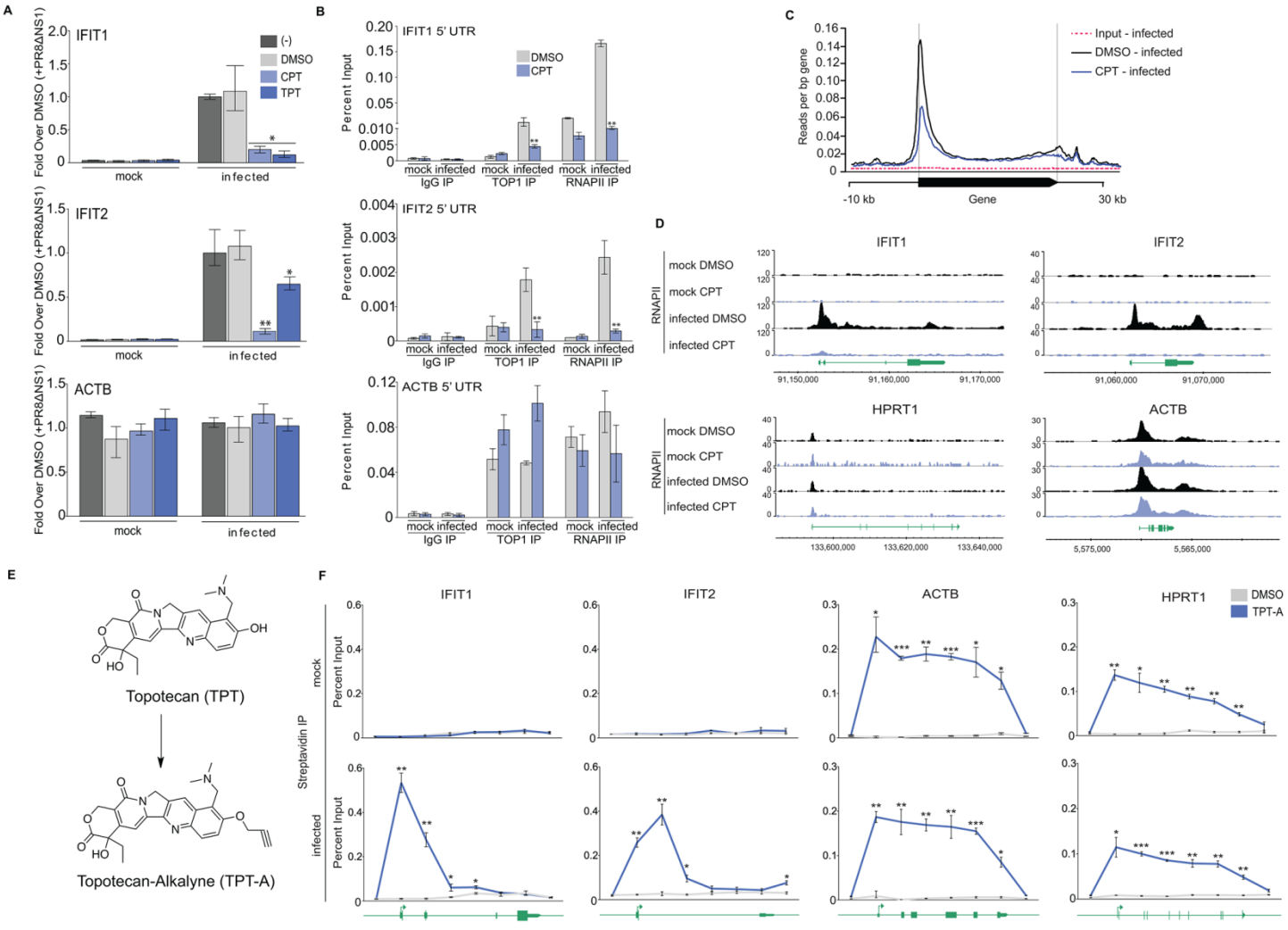

Fig. 2. Topotecan and Camptothecin suppress RNAPII at PAMP-induced genes. (**A**) Gene expression in human A549 cells, left untreated (-) or treated with 0.5 μM of CPT, 100 nM Topotecan (TPT) or DMSO, at 4 hours after mock treatment or PR8ΔNS1 virus infection. (**B**) ChIP-qPCR analysis of endogenous RNAPII and Top1 at the promoters of IFIT1, IFIT2 and ACTB in A549 cells treated with 0.5 μM of CPT or DMSO, at 4 hours after mock treatment or infection with influenza PR8ΔNS1. (**C**) ChIP-seq metaplot of endogenous RNAPII in A549 cells treated with 0.5 μM of CPT or DMSO 6 hours after mock treatment or PR8ΔNS1 virus infection. Plots represent RNAPII occupancy at genes showing a 2-fold upregulation in their expression after infection. (**D**) ChIP-seq tracks of representative antiviral genes IFIT1 and IFIT2, and housekeeping genes ACTB and HPRT1. (**E**) Schematic representation of the chemical synthesis of Topotecan-Alkyne (TPT-A) from TPT. (**F**) Chemical-ChIP qPCR analysis of TPT-A occupancy across IFIT1, IFIT2, ACTB, and HPRT1 genes in A549 cells treated with DMSO or 100 nM TPT-A, at 6 hours after mock treatment or PR8ΔNS1 infection. *P < 0.05, **P < 0.005 and ***P < 0.0005 (calculated with a student's *t* test; with Holm-Bonferroni sequential correction). Data are from three (A) and two [(B) and (F)] independent experiments. Mean and s.d are indicated.

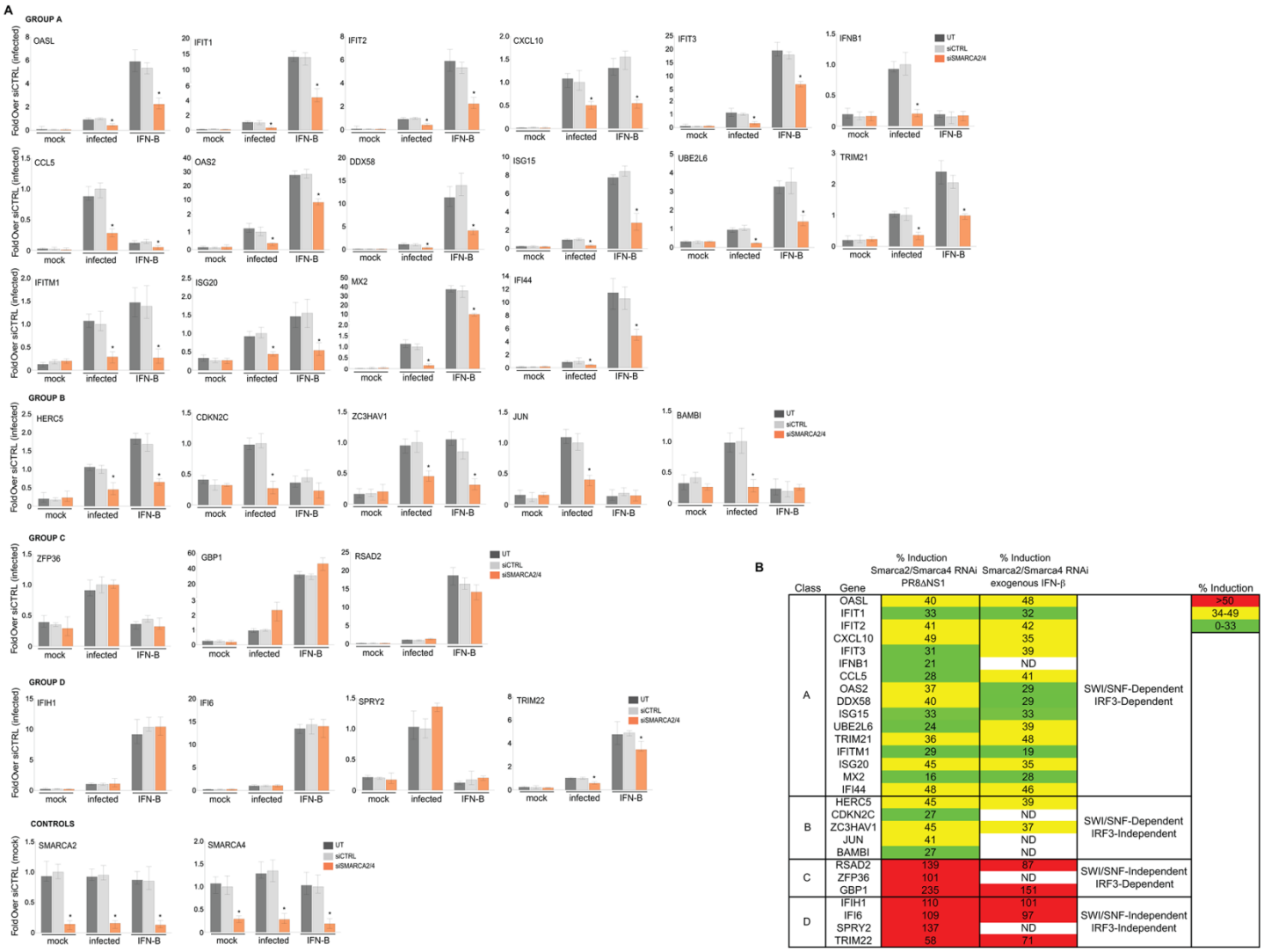

Fig. 3. Classification of SMARCA 2/4 dependent PAMP-induced genes. (**A**) Expression of genes upregulated >2 fold after infection and suppressed by Top1 inhibition in A549 cells at 4 hours after mock treatment, infection with PR8ΔNS1 virus (infected), or stimulation with exogenous IFN-β (IFN-B). Cells were dual-transfected with siRNAs targeting SMARCA2 and SMARCA4 (orange bars). SWI/SNF dependency was evaluated via transient knockdown of SMARCA2/4 and IRF3 dependent genes were compiled from the literature and cross-compared with a list of genes induced by IRF35D in STAT1$^{-/-}$ cells. (**B**) Table summarizing the results for genes in (A). Columns 2 and 3 show the effect of SMARCA2/4 knockdown on PR8ΔNS1 and exogenous interferon (IFN-β)-induced mRNA levels, respectively. Levels of mRNA are shown as a percentage of the mRNA level determined by qPCR in siCtrl-treated A549 cells (set at 100% for each gene). Column 4 classifies the genes: A and B (21/28 genes) are SWI/SNF-dependent (inducibility levels <50%), C and D (7/28) are SWI/SNF-independent (inducibility >50%). Color-coded legends for columns 2 and 3 are shown at the top right. *P < 0.05 (calculated with a student's *t* test; with Holm-Bonferroni sequential correction). Data are from three independent experiments (mean and s.d.).

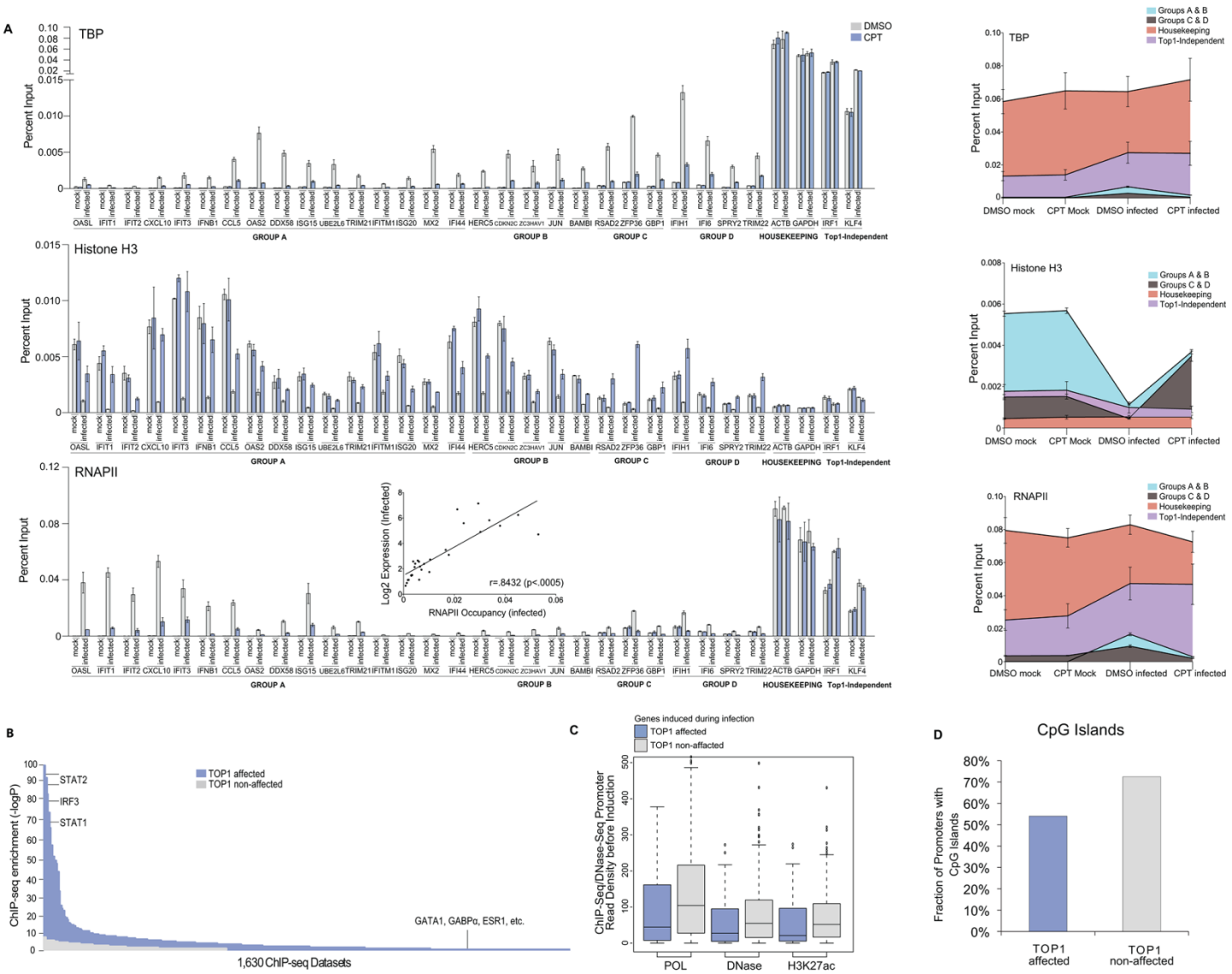

Fig. 4. Top1 inhibition suppresses PAMP-induced genes that require nucleosome remodeling for activation. (**A**) Left, ChIP-qPCR analysis of endogenous TBP, Histone H3, and RNAPII at the promoters of classes A-D, housekeeping, and PAMP-induced Top1-independent genes (IRF1, KLF4) in A549 cells treated with 0.5 μM of CPT or DMSO, at 6 hours after mock treatment or infection with influenza PR8ΔNS1. Right, Summation plots of each individual protein's occupancy (percent input). Inset, correlation plot of gene expression (infected) versus RNAPII occupancy (infected) for genes shown in Fig. 3A. (**B**) 1,630 ChIP-seq datasets were tested for transcription factor (TF) enrichment at the promoters of Top1-affected genes during infection (see methods). Negative log of the P-value of each of these datasets (blue) and results of the same procedure applied to genes unaffected by Top1 depletion (gray). Data shown results from defining promoters as (-1,000,+1) relative to the transcriptional start site. The top 3 TFs and examples of insignificant TFs are shown. (**C**) Basal state meta-analysis of RNAPII (POL) occupancy, DNase hypersensitivity, and H3K27ac occupancy at the promoters of genes designated as either Top1 affected (N = 84) or Top1 non-affected (N = 296) after infection. Data sets used are from ENCODE (see methods) (**D**) Basal state meta-analysis of CpG island occupancy at the promoters of genes designated as either Top1 affected or Top1 non-affected after infection. Data are from two (A) independent experiments. Mean and s.d are indicated.

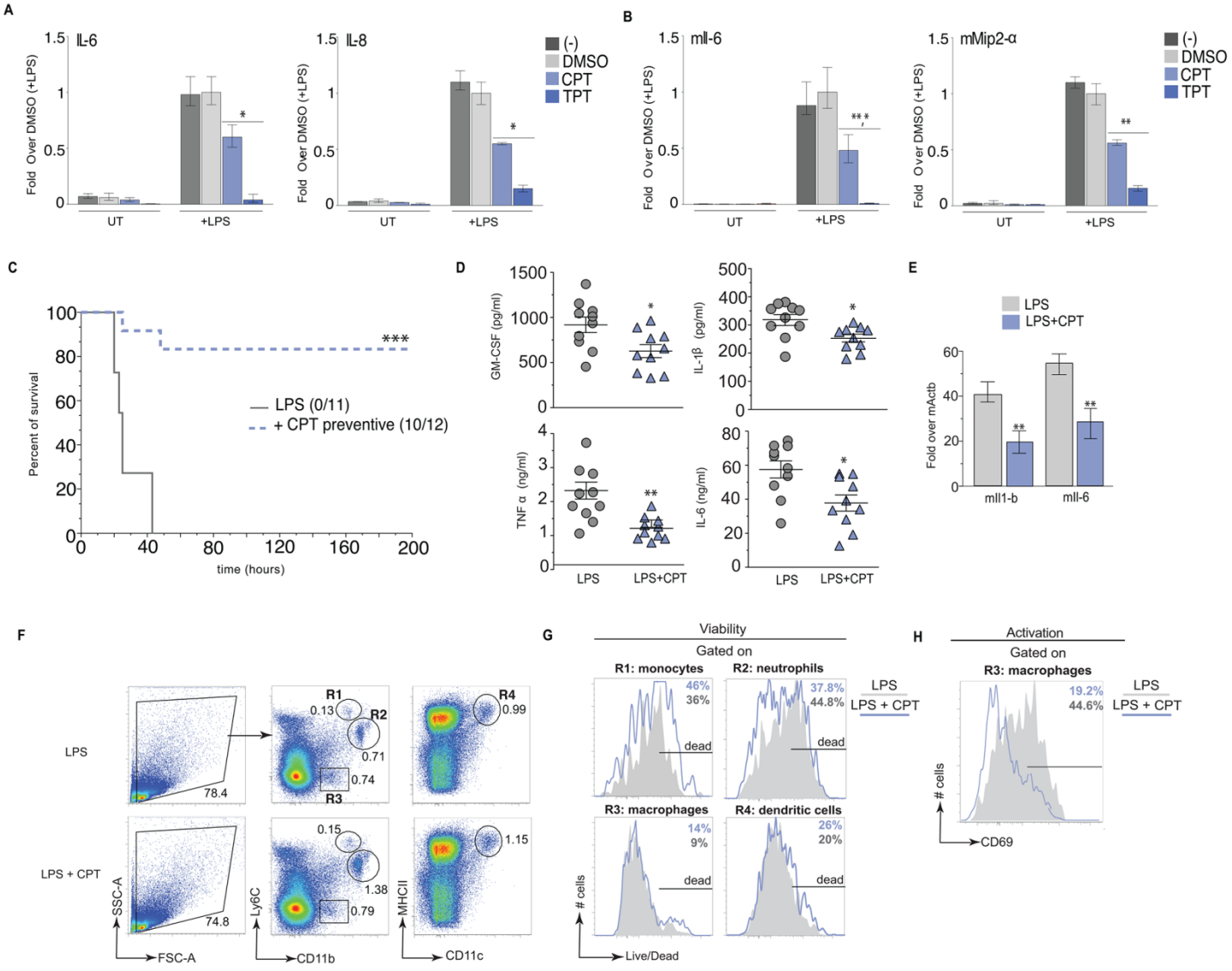

Fig. 5. Top1 regulates LPS-induced inflammation in vitro and in vivo. (**A** and **B**) Gene expression in A549 (A) or RAW 264.7 (B) cells, left untreated (-) or treated with 0.5 μM CPT, 100 nM TPT or DMSO, in the presence of LPS stimulation or not (UT). (**C** to **H**) C57BL/6J mice left untreated or treated with CPT in response to LPS-induced septic shock. (C) Survival curve. (D) Serum titers of indicated cytokines at 4 hours after LPS injection. [(E) to (H)] Ninety minutes after LPS injection spleens were harvested to perform transcriptional analysis of indicated inflammatory genes (E) and to determine cell viability and activation by flow cytometry [(F) to (H)]. (F) Gating strategy. (G) Histograms comparing the incorporation of a Live/Dead dye after gating on R1, R2, R3 and R4. (H) CD69 expression after gating on R3. *P < 0.05, **P < 0.005 and ***P < 0.0005, calculated with a student's *t* test (with Holm-Bonferroni sequential correction) for [(A), (B), (D), (E)] or log rank test (C). Data are from three independent experiments [(A) to (C)] with n = 11 (LPS) and n = 12 (LPS+CPT) individual mice, and two independent experiments [(D) to (H)] with n = 6 (LPS) and n = 7 CPT (LPS+CPT) individual mice. Mean and s.d are indicated.

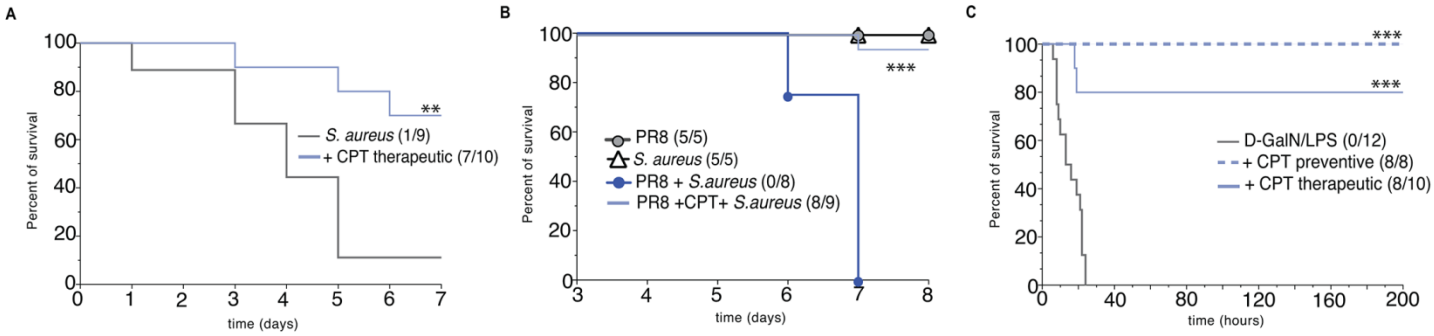

Fig. 6. Top1 inhibition blocks lethal inflammation in vivo. Survival curves of C57BL/6J mice left untreated or treated with CPT in response to *S. aureus* infection (**A**), PR8-*S.aureus* co-infection (**B**) or D-GalN/LPS injection (**C**). Mice were treated with CPT 3, 24 and 48 hours after *S. aureus* infection (A), 12, 24 and 36 after PR8 infection (B) or 2 hours and 30 min after D-GalN/LPS injection. **P < 0.005 and ***P < 0.0005, calculated with a log rank test. Data are from three independent experiments (A) with n = 8 to 12 individual mice, and two independent experiments [(B) and (C)] with n = 5 to 9 individual mice.

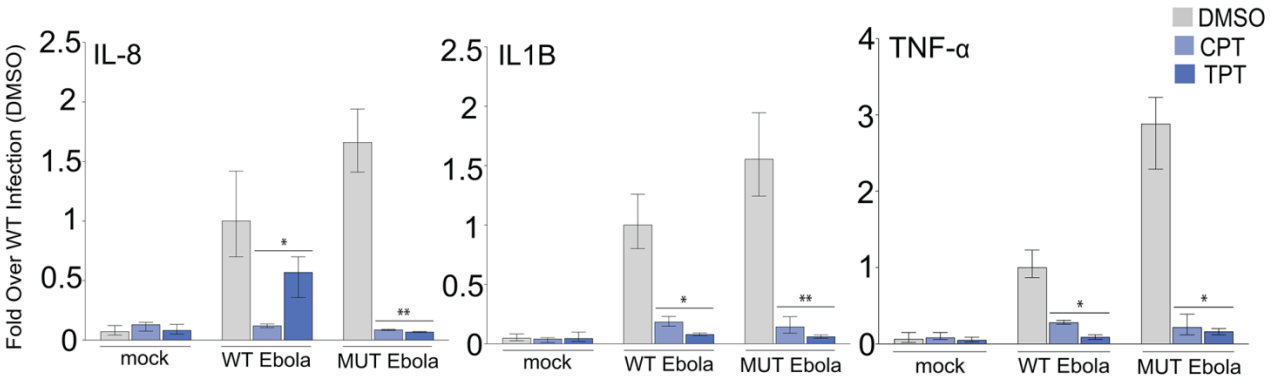

Fig. 7. Suppression of Ebola virus induced inflammation by Top1 inhibitors. THP-1 cells were mock treated or infected with wild-type (WT) Ebola virus (Zaire-Mayinga strain) in the presence of 0.5 μM of CPT, 100 nM of TPT or DMSO. Bar graphs show the relative expression of selected genes. *P < 0.05 and **P < 0.005 fcalculated with a student's *t* test; with Holm-Bonferroni sequential correction. Data are from three independent experiments. Mean and s.d are indicated.

Topoisomerase 1 inhibition suppresses inflammatory genes and protects from death by inflammation

Alex Rialdi, Laura Campisi, Nan Zhao, Arvin Cesar Lagda, Colette Pietzsch, Jessica Sook Yuin Ho, Luis Martinez-Gil, Romain Fenouil, Xiaoting Chen, Megan Edwards, Giorgi Metreveli, Stefan Jordan, Zuleyma Peralta, Cesar Munoz-Fontela, Nicole Bouvier, Miriam Merad, Jian Jin, Matthew Weirauch, Sven Heinz, Chris Benner, Harm van Bakel, Chris Basler, Adolfo García-Sastre, Alexander Bukreyev and Ivan Marazzi (April 28, 2016)

published online April 28, 2016

Editor's Summary

Science (print ISSN 0036-8075; online ISSN 1095-9203) is published weekly, except the last week in December, by the American Association for the Advancement of Science, 1200 New York Avenue NW, Washington, DC 20005.